

Temperature Programmed Infrared and Mass Spectrometry Analysis of Interactions of Covalent Organic Frameworks with Simple Polar and Nonpolar Organic Molecules

A Thesis

submitted to

Indian Institute of Science Education and Research Pune

in partial fulfilment of the requirements for the

BS-MS Dual Degree Program

By

D.V.S.Datta



Indian Institute of Science Education and Research Pune

Dr. Homi Bhabha Road

Pashan, Pune 411008, INDIA

April 2018

Supervisor

Dr. Eric Borguet

Professor, Department of Chemistry

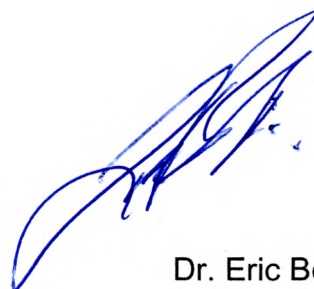
Temple University, Philadelphia, USA

© D.V.S.Datta 2018

All rights reserved

CERTIFICATE

This is to certify that dissertation entitled "**Temperature Programmed Infrared and Mass Spectrometry Analysis of Interactions of Covalent Organic Frameworks with Simple Polar and Nonpolar Organic Molecules**" represents the work carried out by me at the Department of Chemistry, Temple University under the supervision of Dr. Eric Borguet, Professor, Chemistry Department and the same has not been submitted elsewhere for any other degree.



Dr. Eric Borguet

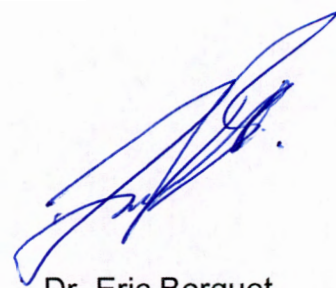


D.V.S.Datta

(20131051)

DECLARATION

I hereby declare that the matter embodied in the report entitled "**Temperature Programmed Infrared and Mass Spectrometry Analysis of Interactions of Covalent Organic Frameworks with Simple Polar and Nonpolar Organic Molecules**" are the results of the work carried out by me at the Department of Chemistry, Temple University, under the supervision of Dr. Eric Borguet, Professor, Chemistry Department and the same has not been submitted elsewhere for any other degree.



Dr. Eric Borguet



D.V.S.Datta

(20131051)

ACKNOWLEDGEMENT

It gives me immense pleasure to thank all those who made this work possible. I would like to thank my advisors, Dr. Eric Borguet and Dr. Ramanathan Vaidhyanathan for their immense support and guidance throughout the project. Their constant motivation and encouragement made me a better researcher and improve my skills.

I would like to thank my lab mates Dr. Melissandre Richard, for motivating me and helping me to become an independent researcher, Isabella Goodenough, Debanjan Chakraborty and Dinesh Mullangi for their immense support throughout the project.

The successful completion of the project wouldn't have been possible without the state-of-the-art facilities provided by Temple University and IISER Pune.

Above all, I would like to thank my parents, especially my mother, P.V. Vijaya Lakshmi, who had trusted me and been supportive to move ahead all through my life.

Dedicated to all the Gurus of my life.

List of tables

Table 1 Synthesis conditions of BCN samples (amounts of chemicals, solvents, temperatures of reaction). ^a 0.3 g CTAB was used in exfoliation of pulp in the synthesis of DVSD04. Sample DVSD03 was synthesized following the reported method [5]	19
Table 2 Summary of synthesized materials, their properties and details.....	22
Table 3 Temperatures of maximum desorption, energies of desorption of acetone, CO ₂ , butane, hexane from COF DC-4 calculated using Redhead analysis	43

List of figures

Figure 1 Synthetic scheme of BCN as reported in ref [5]	11
Figure 2 Connolly representation of IISERP-COF3 [7].....	12
Figure 3 Schematic of hydrogen evolution and oxygen evolution occurring on a photocatalyst [9]	13
Figure 4 Schematic of analyte-sorbent interface at ambient and ultrahigh vacuum conditions respectively. (www.orsayphysics.com).....	14
Figure 5 Schematic of sample holder used for temperature programmed studies	16
Figure 6 Schematic of instrument used for TPD-MS studies.....	16
Figure 7 Schematic of instrument used for TP-IR studies	16
Figure 8 Image of pulp obtained using lab grade tissue paper.....	18
Figure 9 Synthetic scheme of boron carbon nitride	19
Figure 10 Images of obtained samples DVSD-01, DVSD-02, DVSD-03, DVSD-04	20
Figure 11 Sample manipulator with DC-4 coated on the tungsten mesh	24
Figure 12 Image of bakeout of a vacuum chamber using reflective plates and heating tapes (not seen in the image).....	25
Figure 13 Infrared spectra of adsorption of methanol on DC-4 at 100 K, background pressure of 10 ⁻⁹ Torr.....	27
Figure 14 Infrared spectra of temperature programmed desorption of methanol from DC-4, dosed at 100 K and background pressure of 10 ⁻⁹ Torr	28
Figure 15 Infrared spectra of adsorption of methanol on DC-3 at 100 K, background pressure of 10 ⁻⁹ Torr.....	28
Figure 16 Infrared spectra of temperature programmed desorption of methanol from DC-3, dosed at 100 K and background pressure of 10 ⁻⁹ Torr	29
Figure 17 Infrared spectra of adsorption of acetone on DC-4 at 100 K, background pressure of 10 ⁻⁹ Torr.....	30
Figure 18 Infrared spectra of temperature programmed desorption of acetone from DC-4, dosed at 100 K and background pressure of 10 ⁻⁹ Torr	30
Figure 19 TPD-MS spectra of acetone (m/z=43) from DC-4 dosed at 123 K and background pressure of 10 ⁻⁹ Torr	31

Figure 20 Infrared spectra of adsorption of acetone on DC-3 at 100 K, background pressure of 10^{-9} Torr.....	32
Figure 22 Zoom in at 1700 cm^{-1} in the Infrared spectra of temperature programmed desorption of acetone from DC-3, dosed at 100 K and background pressure of 10^{-9} Torr	33
Figure 21 Infrared spectra of temperature programmed desorption of acetone from DC-3, dosed at 100 K and background pressure of 10^{-9} Torr	33
Figure 23 TPD-MS spectra of CO_2 ($m/z = 44$) from DC-4 dosed at 100 K and background pressure of 10^{-9} Torr	34
Figure 24 Infrared spectra of adsorption of CO_2 on DC-4 at 100 K, background pressure of 10^{-9} Torr	35
Figure 25 Infrared spectra of temperature programmed desorption of CO_2 from DC-4, dosed at 100 K and background pressure of 10^{-9} Torr	35
Figure 26 Infrared spectra of adsorption of CO_2 on DC-3 at 100 K, background pressure of 10^{-9} Torr	36
Figure 27 Infrared spectra of temperature programmed desorption of CO_2 from DC-3 dosed at 100 K and background pressure of 10^{-9} Torr	37
Figure 28 Infrared spectra of adsorption of butane on DC-3 at 100 K, background pressure of 10^{-9} Torr.....	38
Figure 29 Infrared spectra of adsorption of hexane on DC-3 at 100 K, background pressure of 10^{-9} Torr.....	39
Figure 30 Infrared spectra of temperature programmed desorption of butane from DC-3 dosed at 100 K and background pressure of 10^{-9} Torr	39
Figure 31 Infrared spectra of temperature programmed desorption of hexane from DC-3, dosed at 100 K and background pressure of 10^{-9} Torr	39
Figure 32 Infrared spectra of adsorption of heptane on DC-4 at 100 K and background pressure of 10^{-9} Torr.....	40
Figure 33 Infrared spectra of temperature programmed desorption of heptane from DC-4, dosed at 100 K and background pressure of 10^{-9} Torr	41
Figure 34 TPD-MS spectra of butane $m/z = 43$ fragment dosed on DC-4 at 123 K and background pressure of 10^{-9} Torr	42
Figure 35 TPD-MS spectra of hexane $m/z = 57$ fragment dosed on DC-4 at 123 K and background pressure of 10^{-9} Torr	42
Figure 36 Infrared spectra of DC-3 on tungsten mesh, used as reference spectra for subtraction, taken at 100 K and base pressure of 10^{-9} Torr.....	46
Figure 37 Infrared spectra of DC-4 on tungsten mesh, used as reference spectra for subtraction, taken at 100 K and base pressure of 10^{-9} Torr.....	47
Figure 38 An example of adsorption of 109 L dosing of an analyte at temperature 110 K and base pressure of 10^{-9} Torr	47
Figure 39 Desorption of MeOH from DC-4, dosed at 110 K and base pressure of 10^{-9} Torr.....	48
Figure 40 Polanyi-Wigner equation to determine rate of thermal desorption.....	48

Figure 41 Final equation of Redhead analysis used to calculate the energy of desorption
..... 49

Contents

Chapter 1: Introduction	11
Section 1: Introduction to 2D materials	11
A. Graphene	11
B. Boron carbon nitride.....	11
C. Covalent organic frameworks (COFs)	12
Section 2: Photoelectrochemical water splitting	13
Section 3: Introduction to surface analysis.....	13
A. Brief description of Ultra-high vacuum (UHV)	14
B. Temperature programmed desorption as a surface analytical technique	15
Section 4: Present work	16
Chapter 2: Materials, methods and experimental conditions	18
Section 1: Synthesis of materials	18
A. Synthesis of Pulp:	18
B. Synthesis of boron carbon nitride using pulp:	18
C. Synthesis of COFs DC-1,2,3	20
D. Synthesis of DC-4	20
E. Synthesis of DC-5	21
Section 2: Description of temperature programmed studies	22
A. Temperature programmed desorption – mass spectrometry	22
B. Temperature programmed– Infrared spectroscopy	23
Section 3: Sample preparation & experimental procedure for temperature programmed desorption studies.....	24
A. Sample preparation.....	24
B. Process of bake out	24
C. Activation of the sample	25
D. Experimental procedure	25
Chapter 3: Results and discussion	26
Section 1: Polar analytes	26
Section 2: Industrially relevant gas: CO ₂	34
Section 3: Nonpolar analytes	37
Chapter 4: Conclusion and future perspectives	44
Chapter 5: References and bibliography	45

Chapter 1: Introduction

Section 1: Introduction to 2D materials

A. Graphene

Graphene is a bidimensional (2D) material which has a hexagonal layer structure. Due to its exceptional optical and electronic properties (conductor), it had a tremendous impact[1] on several fields of science, especially for applications in electrical and semiconductor industry. However, for further/future applications in these industries, tunability of the bandgap is essential, which is not possible with graphene which calls for better materials than graphene.

B. Boron carbon nitride

Boron carbon nitride, referred to as BCN, is a novel hybrid material composed of earth abundant elements and synthesized using readily available and economical precursor sources of boron, carbon and nitrogen. It's structure is similar to that of graphene but is more versatile than it in terms of tunability of bandgap and optical properties [3]

Most of the pioneering research on BCN is being done by the research group of Dr. C.N.R. Rao. Their work suggests that BCN has a multitude of applications ranging from optical to semiconductor to PEC (photoelectrochemical) cells. The remarkable properties of BCN are attributable to its constituent elements boron, carbon and nitrogen, which are similar in sizes but differ in properties. The unusual combination of these three elements renders BCN suitable for various applications [4], and its properties can be tuned based on the elemental ratio in which B, C, and N are combined

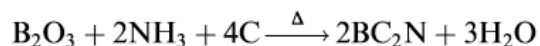
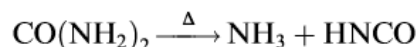
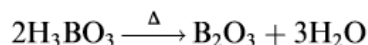


Figure 1 Synthetic scheme of BCN as reported in ref [5]

Inspired by the work of Dr. CNR Rao, we tried to synthesize BCN using a readily available source of carbon: industry grade paper which has 50 – 60 % of carbon by weight. A similar synthetic approach was followed as reported by Dr. CNR Rao (*fig 1*) [5].

C. Covalent organic frameworks (COFs)

Covalent organic frameworks (COFs) belong to the class of crystalline organic polymers, constructed using simple organic units linked together via strong covalent bonds. COFs gained importance very recently and their properties are being explored.

Early works and reports utilized the chemistry of condensation reactions to form COFs containing Boronate and Schiff base linkages [6] (reaction between aldehyde and amine) and yielded corresponding COFs which are robust and stable in various conditions.

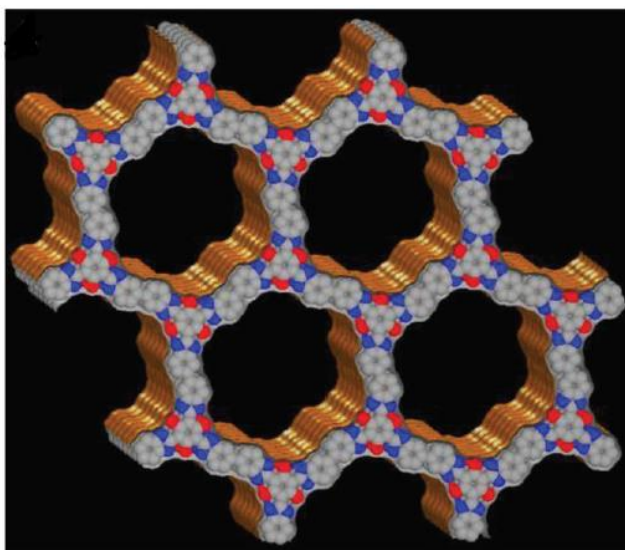


Figure 2 Connolly representation of IISERP-COF3 [7]

Unlike typical polymers, COFs are less dense, form predesigned and predictable crystalline geometries whose porosity can be tuned based on the choice of organic monomer units. Most COFs are synthesized using aromatic rich building blocks, that form planar 2D structures which then stack on one another forming a 3D network (*fig 2*) which renders COFs with high surface areas and porosities [8]. As a result, COFs are promising candidates for applications requiring high surface area and porosity. Moreover, the surface functionalities on the COFs can be readily modified using simple chemistry, which could then catalyze a multitude of reactions [8]

Section 2: Photoelectrochemical water splitting

Photoelectrochemical water splitting has attracted a broad range of research groups as it has the potential of utilizing and converting sunlight (abundant in nature) into chemical energy, generating H_2 , which can be used to meet the increasing energy demands of the growing population in the world. A schematic of water splitting mechanism is shown in the (fig 3)

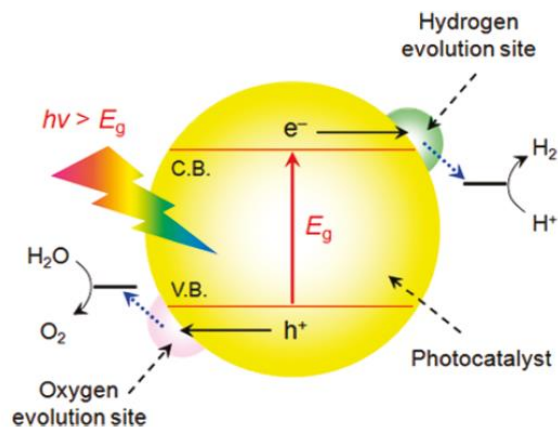


Figure 3 Schematic of hydrogen evolution and oxygen evolution occurring on a photocatalyst [9]

To date, noble metals (Pt) and oxides of some noble metals (IrO_2) have proven to be the best candidates for the water splitting reactions: hydrogen evolution reaction (HER) and oxygen evolution reaction (OER). However, they are prone to photo-corrosion and suffer from issues such as high cost of making and turnover ability.

Recently, alternative materials, were widely explored for their ability to catalyze the water splitting, Some of them which captured a huge attention are 2D layered semi-conducting materials of high surface areas such as TiO_2 [10], BCN [11], MoS_2 [12] Birnessite [13] and their composites [14]. These materials are made up of earth abundant elements and are economical. They are easy to synthesize and modify to be used as photoelectrocatalysts for water splitting. However, the performance of these materials is modest due to the sluggish kinetics of electron transfer processes during water splitting. Hence, major research on developing better photoelectrocatalysts is being carried out to address this issue.

Section 3: Introduction to surface analysis

A. Brief description of Ultra-high vacuum (UHV)

Based on the pressure regimes, vacuum is classified into

- (a) Low vacuum (LV) ($1-1 \times 10^{-3}$ Torr)
- (b) Medium Vacuum (MV) ($1 \times 10^{-3}- 1 \times 10^{-5}$ Torr)
- (c) High vacuum (HV) ($1 \times 10^{-5}- 1 \times 10^{-7}$ Torr)
- (d) Ultra-high vacuum (UHV) ($< 1 \times 10^{-8}$ Torr)

According to the kinetic theory of gases, under ambient temperature and pressure conditions, more than Avogadro number (6×10^{24}) gas particles collide and stick to surface area of 1 cm^2 in second. Hence under these conditions the collision flux, the total number of molecules colliding a surface area of 1 cm^2 in one second will be 6×10^{24} particles/ ($\text{cm}^2 \text{ s}^{-1}$) assuming the sticking probability to be one. Hence the time required for the formation of one monolayer on the surface of the material, which is inversely proportional to collision flux and pressure, is in the order of 1 ns. To increase the time for the formation of monolayer and study the surface phenomena precisely, the monolayer formation time should be increased. This can be achieved by analyzing the materials in ultra-high vacuum and cryogenic conditions (*fig 4*), where most of the kinetic energy of the particles decreases drastically, and the monolayer formation time increases to 10^4 seconds [2] facilitating the study of pristine material devoid of any adsorbed impurities.



Figure 4 Schematic of analyte-sorbent interface at ambient and ultrahigh vacuum conditions respectively. (www.orsayphysics.com)

There are specialized vacuum pumps used to generate ultra-high vacuum and they are:

- (a) Ion pump
- (b) Cryogenic pumps
- (c) Turbo molecular pumps
- (d) Diffusion pumps

In the present work, a turbo molecular pump is used to generate ultra-high vacuum. Turbo molecular pumps are efficient in generating ultra-high vacuum compared to others [15]. Also, they can be started and stopped in under an hour. The turbo molecular pump is backed by a mechanical pump which is connected to the system, to maintain the outlet pressure of the turbo molecular pump below 100 mTorr.

B. Temperature programmed desorption as a surface analytical technique

Temperature programmed desorption (TPD) is an experimental technique widely used in the field of surface analysis and catalysis. This technique allows one to study the interaction of gases/analytes of interest with material surfaces and examine the active/binding sites. TPD experiments provide an insight into the mechanism of adsorption, desorption that occurs on the solid surfaces and explore the possibilities of any surface reactions that could take place when the material interacts with the analyte of interest. Moreover, reactions that are temperature dependent can be studied using TPD technique and the kinetics of such reactions can be monitored and enhanced [16]. These examples prove that TPD can be effectively utilized in various fields of science

Many theories like Redhead analysis, leading edge and complete analysis have been developed to calculate the energy of desorption of the gas molecules on the solid surfaces. The effectiveness and versatility of TPD experiments have been reported in the Borguet group. In a typical TPD experiment, a small amount of the sample is directly placed in a vacuum chamber. The analyte of interest is then allowed to interact and equilibrate with the material, adsorb on to the surface of the material. The sample is then heated up gradually, at a programmable linear rate and the desorbed species are monitored as a function of temperature and time. Detection of desorbed species is made using mass spectrometer (MS), and detection of surface bound species can be made using Fourier transform infrared (FTIR) spectrometer.

In the Borguet group, TPD-MS and FTIR were extensively used to study carbonaceous materials such as SWCNT [17], HOPG [18] and their interactions with simple polar (acetone), non-polar (propane, n-heptane) and industrially relevant gases (CO₂, NH₃). Especially the studies conducted on SWCNT suggest that molecules adsorbed endohedrally have the effective IR cross section reduced compared the molecules

adsorbed exohedrally. This leads to the idea of shielding/screening of molecules in SWCNT [19].

A schematic of sample holder (fig 5), TPD-MS (fig 6), TP-IR (fig 7) used in the following study are shown below.

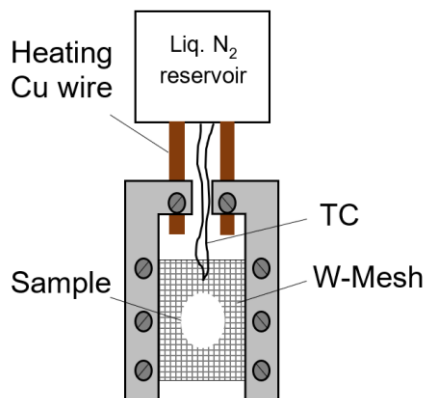


Figure 5 Schematic of sample holder used for temperature programmed studies

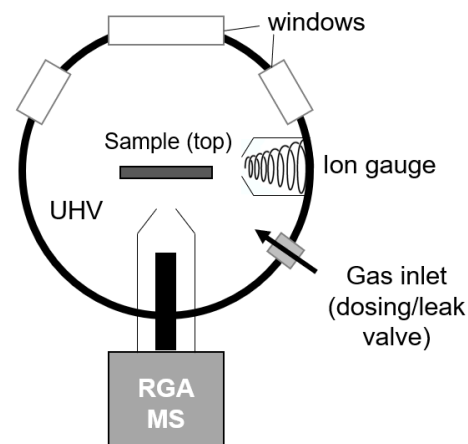


Figure 6 Schematic of instrument used for TPD-MS studies

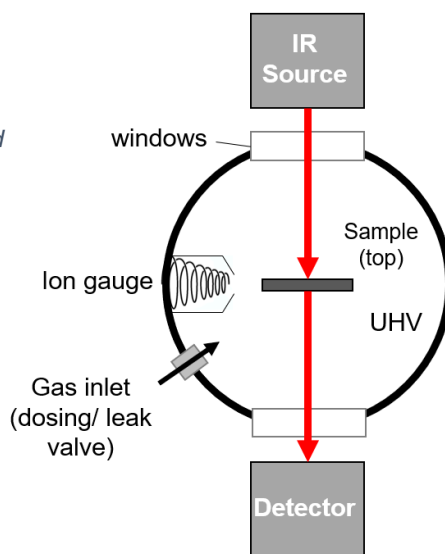


Figure 7 Schematic of instrument used for TP-IR studies

Section 4: Present work

The ultimate goal of our study was to understand how water splitting occurs on the surfaces of our materials by determining

- (a) mechanisms of adsorption and desorption,

(b) specificity and selectivity in interactions between water and metal nanoparticles and their clusters,

(c) the role of BCN, COF as a system by itself and as a support for metal nanoparticles (MNPs) to catalyze the photoelectron chemical water splitting.

However, water is very hard to pump out of the vacuum chamber, a lot of energy and time are required to get rid of excess water in the system. Hence as a first step, the work presented here encompasses the synthesis of BCN and COFs (DC-1, DC-2, DC-3, DC-4, DC-5), study and analysis of interactions of, COFs (DC-3, DC-4), with chief industrial analytes (CO_2), some simple polar and non-polar laboratory chemicals (acetone, hexane) and molecules whose chemical properties are similar to water (methanol). The results will give an insight into the basic processes like adsorption, desorption occurring in these materials and help to make improvements and design superior materials for water splitting applications.

Chapter 2: Materials, methods and experimental conditions

Section 1: Synthesis of materials

A. Synthesis of Pulp:

Pulp was synthesized by soaking lab grade tissue paper, in a 1:1 mixture of Dimethyl Formamide (DMF) and H₂O. This was done to exfoliate the fibers of the paper. The solution was stirred for 15 mins and left undisturbed for 2 days. The resulting exfoliated pulp was taken out by draining the liquid mixture into appropriate waste container. The pulp was allowed to dry and was grinded into tiny bits using a household grinder. The resulting material was used as a source of carbon (*fig 8*). After many hit and trials, 5 g of pulp was found to be the minimum amount of pulp required to form some visible remnants in the reaction crucible after the reaction is performed.



Figure 8 Image of pulp obtained using lab grade tissue paper

B. Synthesis of boron carbon nitride using pulp:

Pulp was taken in a 100 ml round bottom (RB) flask and sufficient amount of water was added to it. The RB flask was sonicated for 20-30 mins and the contents are transferred to a high temperature crucible and thoroughly mixed with boric acid and urea. Prior to the addition of urea and boric acid they were grinded together in a mortar and pestle to

enhance the surface area of the reaction. After sonication, the liquid was evaporated in a rotary evaporator. Water was added to the reaction crucible and the resulting mixture was warmed at 333 K (393 K in the case of DVSD04) to form a thick slippery liquid and then the crucible was heated in a tube furnace at 1173 K for 10 hours under N₂ atmosphere. After cooling to room temperature, the reaction mixture was heated in an excess urea medium at 1203 K for 3 hours. A schematic of synthetic procedure of BCN is shown in (fig 9)

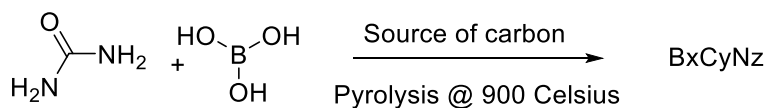


Figure 9 Synthetic scheme of boron carbon nitride

The amounts of pulp, urea, and other chemicals utilized for the synthesis of BCN, are reported in Table 1.

Pulp (g)	Boric acid (g)	Urea (g)	MeOH (mL)	H ₂ O (mL)	Sonication time (hrs)	Drying temperature (K)	Pyrolysis temperature (K)	Name of sample obtained
2	0.3	3.6	0	40	1	333	553	None
5	0.3	3.6	0	40	1	333	1173	DVSD-01
5	0.3	3.6	40	40	1	333	1173	DVSD-02
5	0.3	3.6	40	40	2	393	1173	DVSD-04 ^a

Table 1 Synthesis conditions of BCN samples (amounts of chemicals, solvents, temperatures of reaction). ^a 0.3 g CTAB was used in exfoliation of pulp in the synthesis of DVSD04. Sample DVSD03 was synthesized following the reported method [5]



Figure 10 Images of obtained samples DVSD-01, DVSD-02, DVSD-03, DVSD-04

The reactions yielded black powder as seen in (fig 10). Many variations in the composition of precursors and synthetic scheme were done to obtain porous BCN. CTAB was used in case of DVSD-04 to exfoliate the pulp.

The obtained samples were activated at 393 K overnight before performing any adsorption or BET studies.

C. Synthesis of COFs DC-1,2,3

The COFs DC-1,2,3 are synthesized following a reported method [8]

2,4,6-Tris(p-formylphenoxy)- 1,3,5-triazine (100 mg, 0.23 mmol), 1,4 diaminobenzene (48 mg, 0.46 mmol), were dissolved in 5 mL of 1,4 dioxane. 5 mL of mesitylene was added to the reaction and the contents were homogenized by stirring. Later, 0.5 mL of 3 M acetic acid was added and the Pyrex tube was flash frozen in liquid nitrogen bath. The empty space in the Pyrex tube was evacuated and the tube was sealed by maintaining N₂ atmosphere. The tube was placed in oven and the temperature was maintained at 393 K.

D. Synthesis of DC-4

DC-4 has been synthesized by following similar method as reported in [8] but 1,4 diaminobenzene is replaced with hydrazine. 2,4,6-Tris(p-formylphenoxy)- 1,3,5-triazine (100 mg, 0.23 mmol), hydrazine (15 mg, 0.46 mmol), were dissolved in 4 mL of 1:1 mixture of mesitylene and ortho dichloro benzene. To the reaction mixture 4 mL of ethanol was added, and the contents were homogenized by stirring. Later, 0.5 mL of 3 M acetic acid was added and the Pyrex tube was flash frozen in liquid nitrogen bath. The empty space in the Pyrex tube was evacuated and the tube was sealed by

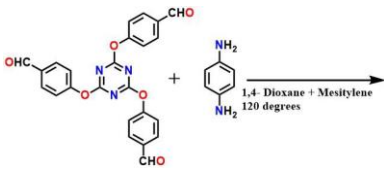
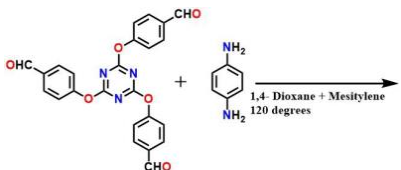
maintaining N₂ atmosphere. The tube was placed in oven and the temperature was maintained at 393 K.

E. Synthesis of DC-5

DC-4 (500 mg) was thoroughly mixed in a 20 mL aqueous solution of boric acid (0.15 g) and urea (1.8 g). The mixture was warmed at 60 °C to form a thick slippery liquid which was dried at the same temperature. The dried mixture was transferred to a crucible and placed in a tube furnace. The tube furnace was heated to 1173 K for 10 hours under N₂ atmosphere. After cooling the contents to room temperature, the resulting powder was heated to 1203 K for 3h in an excess urea atmosphere.

The resulting COFs and BCN were activated at 393 K overnight before performing any adsorption and BET studies. This approach yielded us a crystalline BCN compared to the previous method.

Table 2 summarizes the synthetic scheme, BET surface area, solvents used to disperse the COFs.

Name of the material	Synthetic scheme and properties	Solvent(s) to disperse the COF	BET surface area
DC-1	<ul style="list-style-type: none"> Synthetic scheme; reaction time: 3 days Pore size = 22 Å 	THF, EtOH	408.5 m ² /g
DC-2	<ul style="list-style-type: none"> Synthetic scheme; reaction time: 5 days 	THF, EtOH	408.5 m ² /g
DC-3	<ul style="list-style-type: none"> Synthetic scheme; reaction time: 7 days 	THF, EtOH	408.5 m ² /g

DC-4	<ul style="list-style-type: none"> • Synthetic scheme • Pore size = 22 Å • reaction time: 7 days 	THF, EtOH, DMF	2000 m ² /g
DC-5 (BCN)	<ul style="list-style-type: none"> • Synthetic scheme mentioned above • Size of major pore= 12 Å 	THF, EtOH	180m ² /g

Table 2 Summary of synthesized materials, their properties and details

Section 2: Description of temperature programmed studies

A. Temperature programmed desorption – mass spectrometry

Temperature Programmed Desorption coupled to Mass Spectrometer (TPD-MS) detection system is used to study the chemical species that desorbs from the surface of materials upon heating at a known rate. Using this technique, we can obtain the following information:

- Identification of masses of molecular fragments desorbing from the surface upon heating
- Detect the presence of multiple adsorption sites, for adsorbed gas molecules, on the materials (presence of multiple peaks during the desorption)
- Determine the energy of adsorption of each adsorption site present on the material
- Determine the kinetics of desorption process
- Detect any irreversible transformations taking place, upon adsorption and during desorption, on the surface of the material

The TPD-MS experiments are performed in a stainless-steel vacuum chamber, designed and developed in the Borguet group. The chamber is pumped by a turbo molecular pump (Leybold turbovac 151) backed by a mechanical pump provides a base pressure in the range 10^{-9} – 10^{-10} Torr after bakeout. A tungsten (W) mesh (AlfaAesar,

100 mesh, 150 x 150 mm, 0.001-inch wire diameter) is cut into a 1.0 x 0.5 in rectangular mesh. The tungsten mesh is connected to copper wires fixed by nickel clamps. The sample manipulator is cooled down using a liquid nitrogen dewar which allows cooling of the samples to cryogenic temperatures (100 K). Heating up to 1400 K is possible and has been reported. However, heating up to 473 K was performed in our experiments, keeping in mind the stability of the materials that have been used. Gases are dosed onto the material at cryogenic temperatures by backfilling the chamber through a leak valve (Varian and Duniway).

After the desired dosage is completed, the pressure in the chamber is allowed to recover to base pressures, TPD spectra are recorded while heating the material at a constant ramp rate (usually 2 K/s). The pressures inside the chamber are monitored using an ion gauge. To heat the sample, direct current from AEHR (10- 100) is driven through the W-mesh. Temperature of the W mesh is monitored and controlled using a K-type thermocouple spot welded to W- mesh. Residual gas analyzer (RGA 300 Stanford Research systems) is used to monitor the masses of the desorbed species. Custom made LabVIEW programs were used to control and monitor temperature, dosing and record the TPD-MS profiles.

B. Temperature programmed– Infrared spectroscopy

Infrared spectroscopy was used to study the temperature dependent changes in surface functionalities of the sample and identify changes in vibrational modes of the sample/ adsorbed molecules. A stainless-steel vacuum chamber was used to record FTIR spectra under UHV conditions. The vacuum chamber is positioned into the sample compartment of a Bruker Optics Tensor 27 series FTIR spectrometer, which is coupled to a DTGS (Deuterated TriGlycine Sulfate) detector operational in the region 12000 cm^{-1} - 400 cm^{-1} . In this work, all our spectra were recorded in the region: 4000 cm^{-1} - 400 cm^{-1} with a resolution of 4 cm^{-1} . The design of the sample holder used in FTIR studies is similar to the sample holder used in TPD-MS studies and allowed a cooling of the samples to cryogenic temperatures (100 K). Heating up to 1400 K can be achieved but considering the sample stability temperatures up to 473 K were employed in the interest of sample's stability. The sample manipulator used for the infrared studies rests on a Z stage which is used to adjust the relative height of the sample with reference to the infrared beam. The height of the sample is set accordingly to maximize the interaction between sample and the infrared beam. In our experiments, the background is bare tungsten mesh. The reference spectra are the infrared spectra of COF, coated on the tungsten mesh, taken at 100 K (see appendix for further information). During the analysis, all adjustments to the infrared spectra, manual baseline correction and spectrum subtraction, were applied using Bruker OPUS software

Section 3: Sample preparation & experimental procedure for temperature programmed desorption studies

A. Sample preparation

To carry out the temperature programmed studies, the synthesized COFs DC-3 and DC-4 were loaded onto the tungsten mesh. To coat the sample on the tungsten mesh, roughly 10-20 mg of the sample is taken and dispersed in a suitable solvent (usually DMF or EtOH) and sonicated for 10-15 mins. Then the sample is centrifuged for 10 mins @ 8000 rotations per minute. The supernatant is drained off carefully, using a pipette, without disturbing the sample. The sample is then coated uniformly on the tungsten mesh as shown in *fig 11*. To prevent quick drying of the sample on the tungsten mesh, the choice of solvent is made in such a way that the solvent takes some time to evaporate and sample adheres to the tungsten mesh (*fig 5,6*). The entire sample manipulator is then taken carefully and inserted into the vacuum chamber sealed using a copper gasket.



Figure 11 Sample manipulator with DC-4 coated on the tungsten mesh

To ensure appropriate connectivity of the tungsten mesh to the sample manipulator (*fig 5*), and avoid other unnecessary connections, the sample is tested for proper functioning of the ramp rate and connections, prior to bake out, by generating ultrahigh vacuum and cooling down to roughly between 100 K and 120 K and flash heating to 473 K at 2 K/s.

B. Process of bake out

Generally stainless-steel chambers are baked out in the temperature range 323 K – 373 K to get rid of moisture and contaminants adsorb in the parts of the chamber when it

was opened to atmosphere. To achieve an effective pumping out of the adsorbed impurities, bakeout into turbo molecular pump is done. All the electrical connections and heat sensitive materials are excluded before starting the bake out process. Reflective plates are used to cover the entire chamber, which have electrical connections, to facilitate heating of vacuum the chamber. Heating tapes are also used to achieve uniform heating of the chamber (*fig 12*). To maintain required temperature and prevent heat loss to atmosphere, the reflective plates are insulated with Aluminum (Al) tape. The temperature of the system at various spots of the system is monitored using thermocouples for every 15 mins for the first one hour and the bakeout is continued for 18 - 24 hours.



Figure 12 Image of bakeout of a vacuum chamber using reflective plates and heating tapes (not seen in the image)

C. Activation of the sample

After the bakeout process, the entire vacuum chamber is allowed to cool down to room temperature. All the electrical connections are appropriately made then the IR chamber is moved back into the IR cell and aligned. The detector residual gas analyzer is connected to the TPD-MS chamber and the pressure is monitored. Activation of samples is performed in order to obtain a clean surface of the material and make sure that the material is ready to interact with the analyte of interest. All the samples are activated to 473 K for 1 hour and changes in the sample and the system are monitored.

D. Experimental procedure

- The analyte of interest is taken in a dosing flask and connected to the gas line to which the leak valve is also connected. Freeze thaw of the analyte is performed to increase the purity of the analyte present in the dosing flask.
- **Adsorption of analyte:**
 - The sample is cooled to cryogenic temperatures using liquid N₂
 - Leak valve, attached to the vacuum chamber where the sample is present, allows a specific amount/dosing of analyte to interact with the sample. The desired Langmuir dose was performed by opening the leak valve for a prescribed amount of time. (1 Langmuir = 10⁻⁶ Torr-second) (refer appendix for detailed calculations)
 - After the required dosage of analyte is performed, the leak valve is closed and the pressure inside the chamber is allowed to restore to the background/base pressure.
- **Desorption:**
 - The sample is flash heated from 100 K to 473 K at 2 K/s.

IR spectra and mass spectra were recorded in the TP-FTIR and TPD-MS chambers respectively during adsorption and desorption processes.

Chapter 3: Results and discussion

Section 1: Polar analytes

Methanol and acetone are chosen as polar analytes, to study their interactions with DC-3 and DC-4. The interactions of acetone with various carbonaceous materials was studied in the Borguet group and different adsorption sites for acetone adsorption on CNT were revealed.

- A. There appears to be no interaction of methanol with either DC-3 or DC-4.
 - **DC-4:** Infrared spectra of adsorption of methanol on DC-4 (*fig 13*), shows no evidence of adsorption as the expected peaks for methanol in the region 3500- 3000 cm⁻¹ are absent. Also, the infrared spectra (*fig 14*), mass spectra (*fig 36; appendix*), taken during temperature programmed desorption of methanol suggests no interaction with DC-4

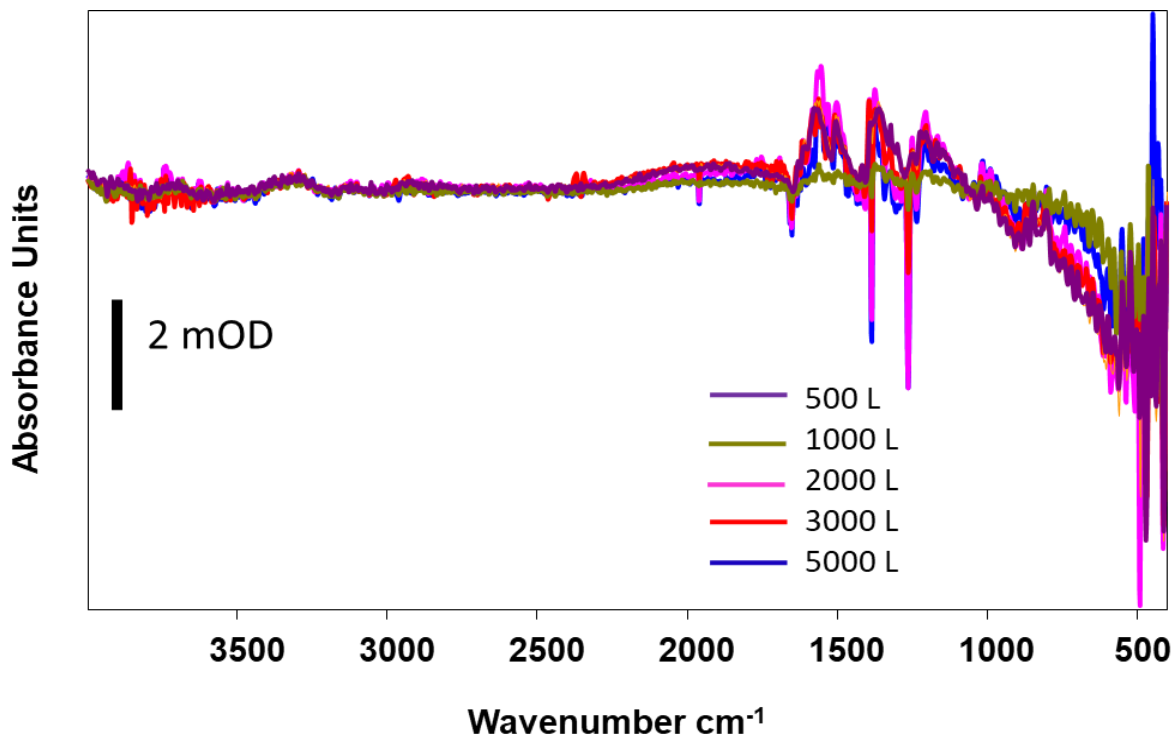


Figure 13 Infrared spectra of adsorption of methanol on DC-4 at 100 K, background pressure of 10^{-9} Torr

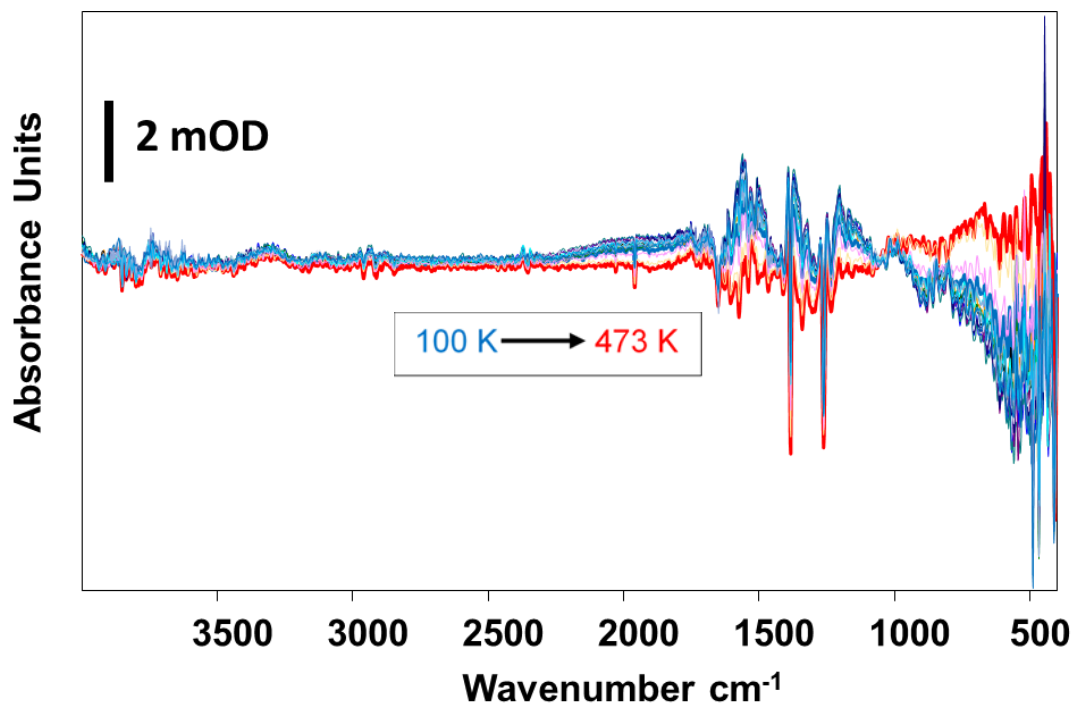


Figure 14 Infrared spectra of temperature programmed desorption of methanol from DC-4, dosed at 100 K and background pressure of 10^{-9} Torr

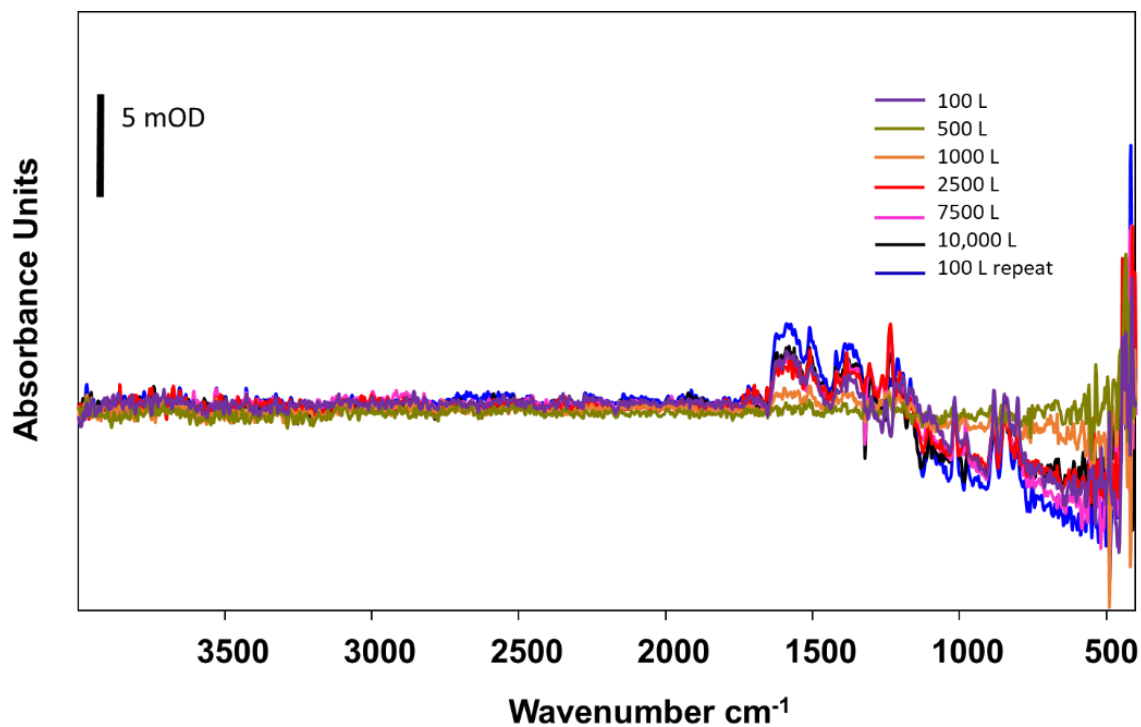


Figure 15 Infrared spectra of adsorption of methanol on DC-3 at 100 K, background pressure of 10^{-9} Torr

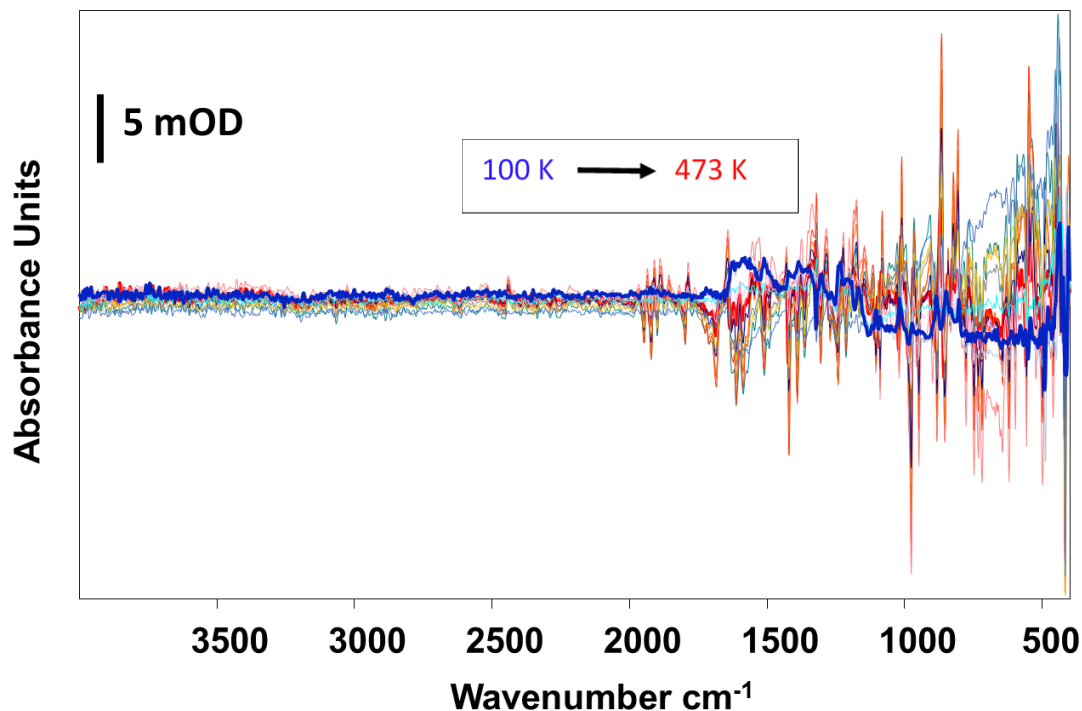


Figure 16 Infrared spectra of temperature programmed desorption of methanol from DC-3, dosed at 100 K and background pressure of 10^{-9} Torr

- DC-3:** Infrared spectra of adsorption (*fig 15*) and temperature programmed desorption (*fig 16*) of methanol on DC-3 show no sign of methanol interaction with DC-3.
 Hence, we conclude that the COFs DC-3 and DC-4 are not very good sorbents for methanol. We speculate that methanol passes through the pores of DC-3 and DC-4 without any affinity to the framework.

B. Acetone shows considerable interactions with DC-3 and DC-4.

- DC-4:** The infrared spectra taken during adsorption (*fig 17*) and temperature (*fig 18*) programmed desorption of acetone, show no peaks corresponding to acetone.

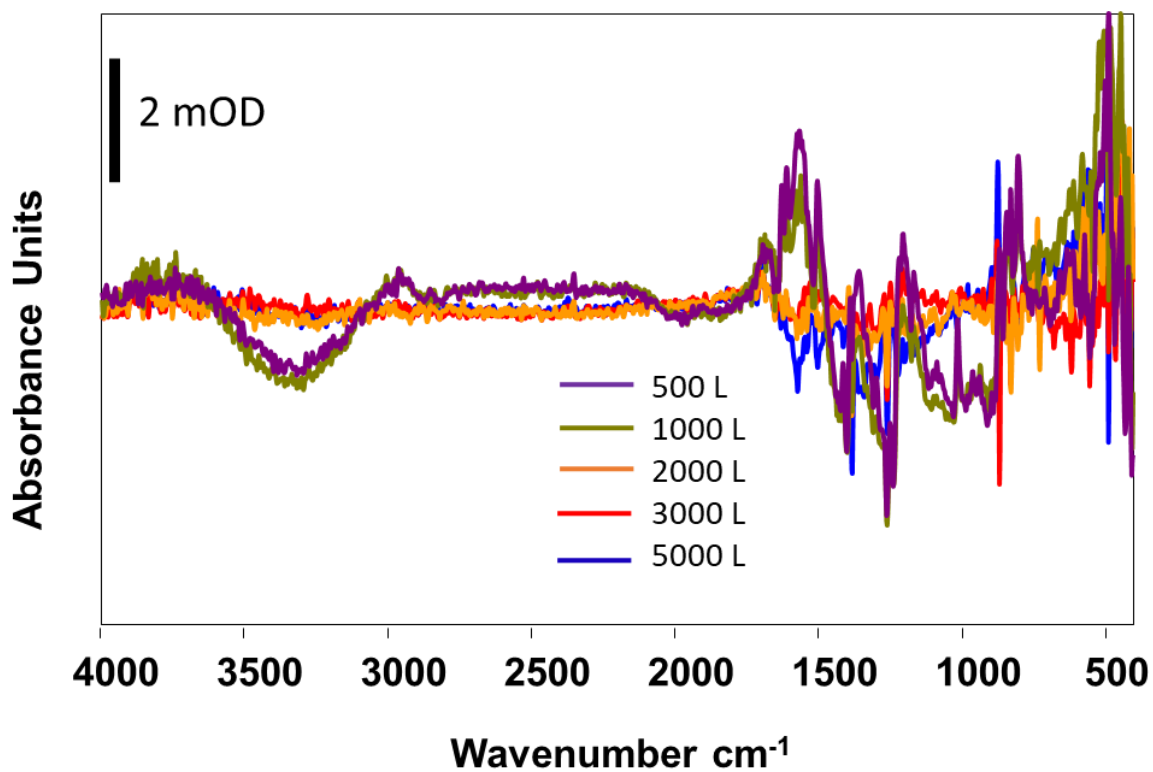


Figure 17 Infrared spectra of adsorption of acetone on DC-4 at 100 K, background pressure of 10^{-9} Torr

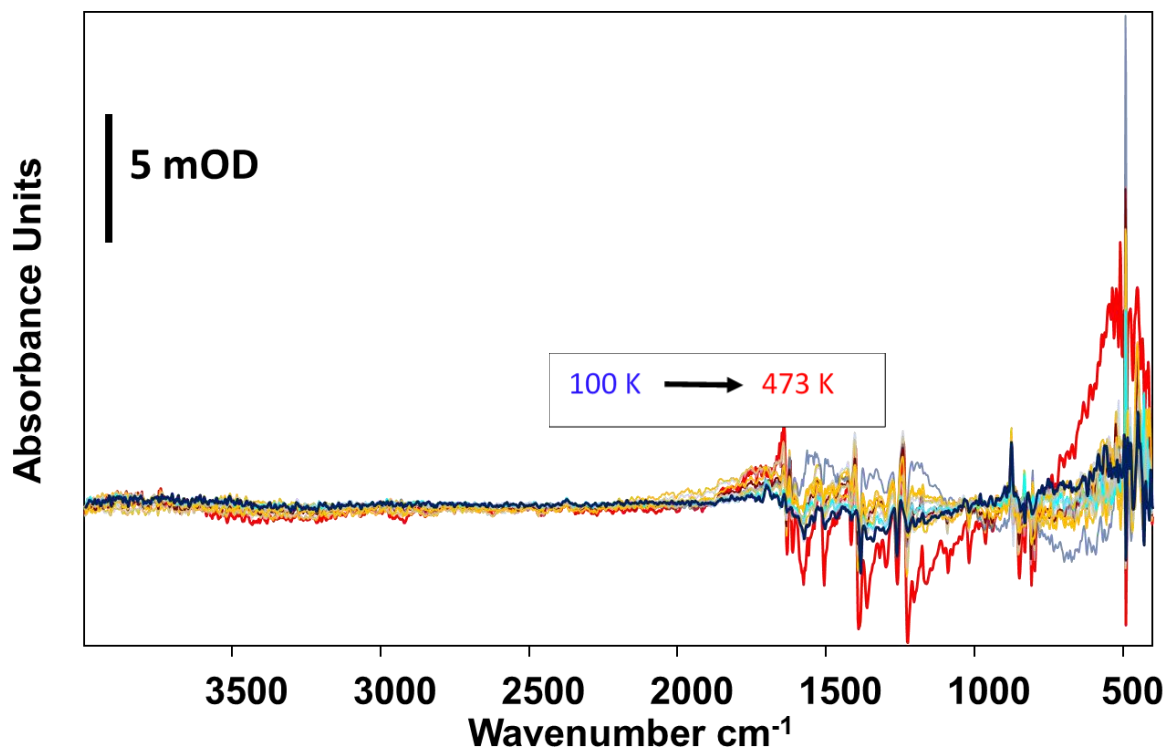


Figure 18 Infrared spectra of temperature programmed desorption of acetone from DC-4, dosed at 100 K and background pressure of 10^{-9} Torr

- These results suggest no interaction of acetone with DC-4. However, mass spectra taken during the temperature programmed desorption of acetone from DC-4 contradicts the above results (*fig 19*). Clearly, the desorption intensity of mass fragment $m/z=43$ (CH_3O^+), which is the base peak in the mass spectrum of acetone, increases with dosing. We observe that desorption spectra for various dosing of acetone share a common leading edge and the maximum temperature of desorption (T_{max}) is found to be 155 K. Also, a shoulder peak at 175 K becomes prominent as the dosing of acetone increases more than 3500 L. The energies of desorption of acetone are found to be using the redhead analysis (described in appendix) and reported in *Table 3*. The two different peaks in the mass spectra suggests the presence of multiple binding sites with different binding energies.

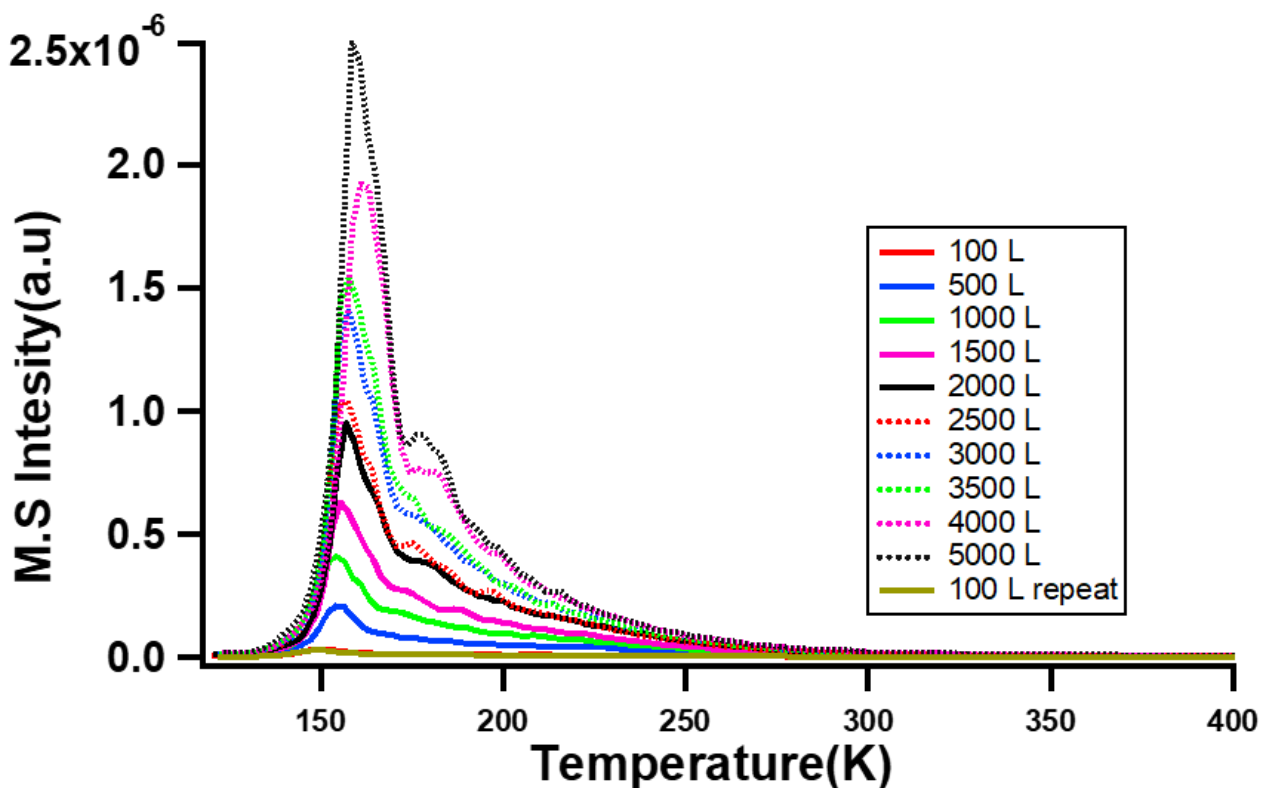


Figure 19 TPD-MS spectra of acetone ($m/z=43$) from DC-4 dosed at 123 K and background pressure of 10^{-9} Torr

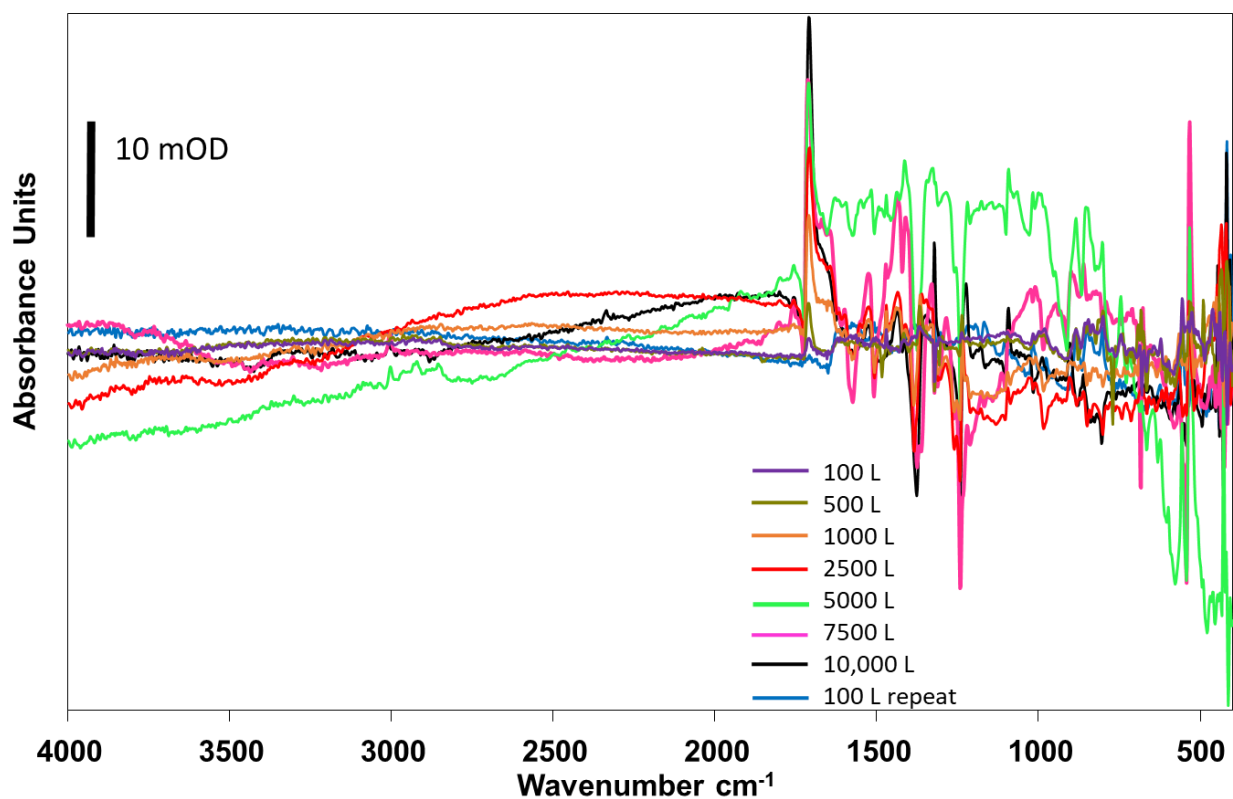


Figure 20 Infrared spectra of adsorption of acetone on DC-3 at 100 K, background pressure of 10^{-9} Torr

- DC-3:** The infrared spectra of adsorption of acetone on DC-3 (fig 20) show the carbonyl stretching at 1700 cm^{-1} whose peak intensity increases with dosing. After 10,000 L dosing, DC-3 was dosed with 100 L of acetone to check for any changes occurring in DC-3 due to the adsorption. It is clear from the above spectra that acetone adsorption on DC-3 is reversible which is also seen in the infrared spectra taken during the temperature programmed desorption (fig 21A, 21B).

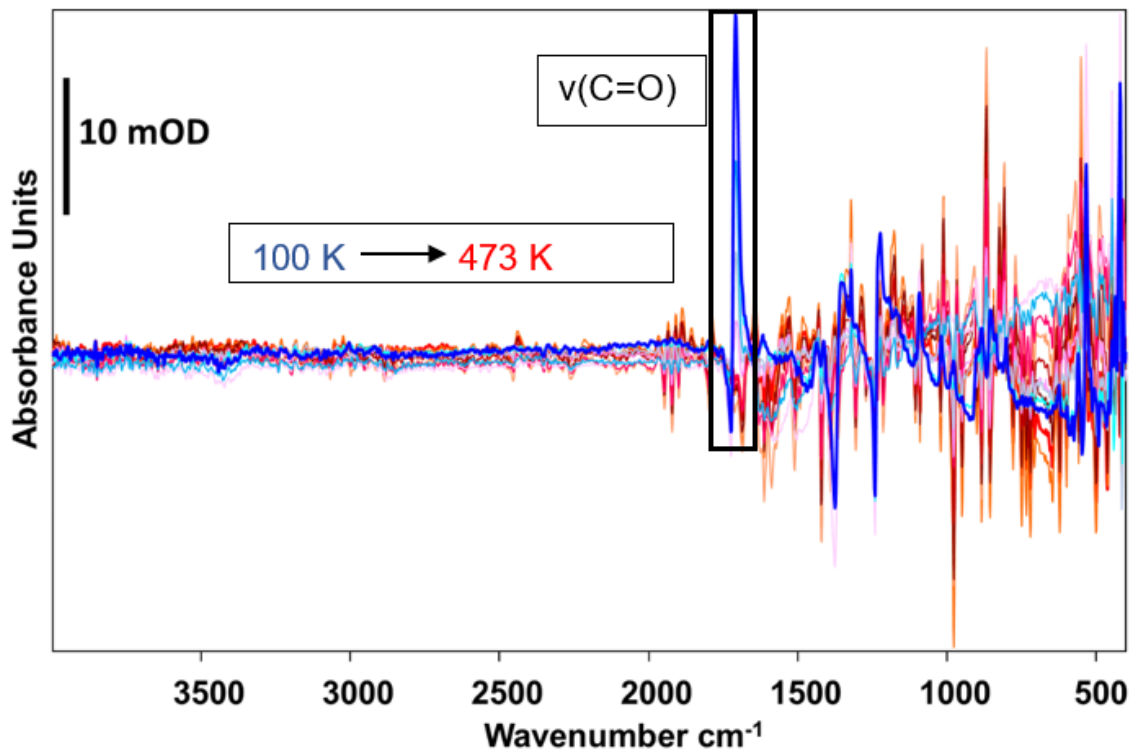


Figure 22 Infrared spectra of temperature programmed desorption of acetone from DC-3, dosed at 100 K and background pressure of 10^{-9} Torr

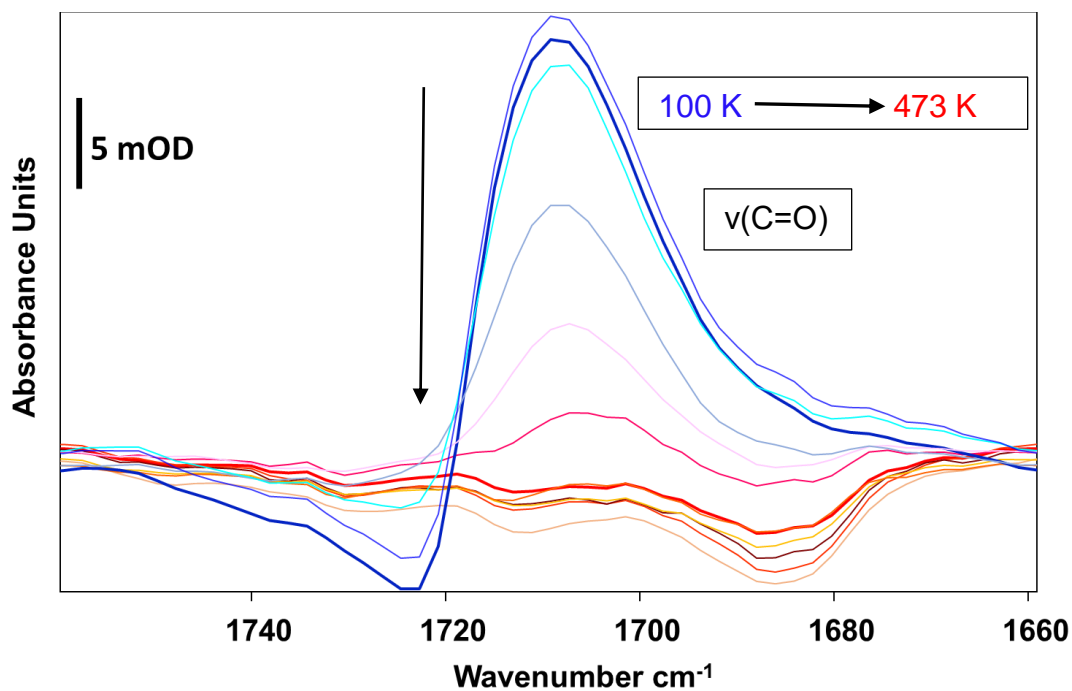


Figure 21 Zoom in at 1700 cm⁻¹ in the Infrared spectra of temperature programmed desorption of acetone from DC-3, dosed at 100 K and background pressure of 10^{-9} Torr

Section 2: Industrially relevant gas: CO₂

CO₂ is a very important industrial gas, which also has a huge impact on the environment. Also, temperature programmed studies of CO₂ can be correlated to BET isotherms of the material. Hence, we studied the interactions of CO₂ with DC-3 and DC-4

- **DC-4:** Mass spectra are taken during temperature programmed desorption of CO₂ from DC-4 (*fig 23*). Very little desorption is seen at the temperature 126 K. The energies of desorption are calculated using Redhead analysis and reported in *Table 3*

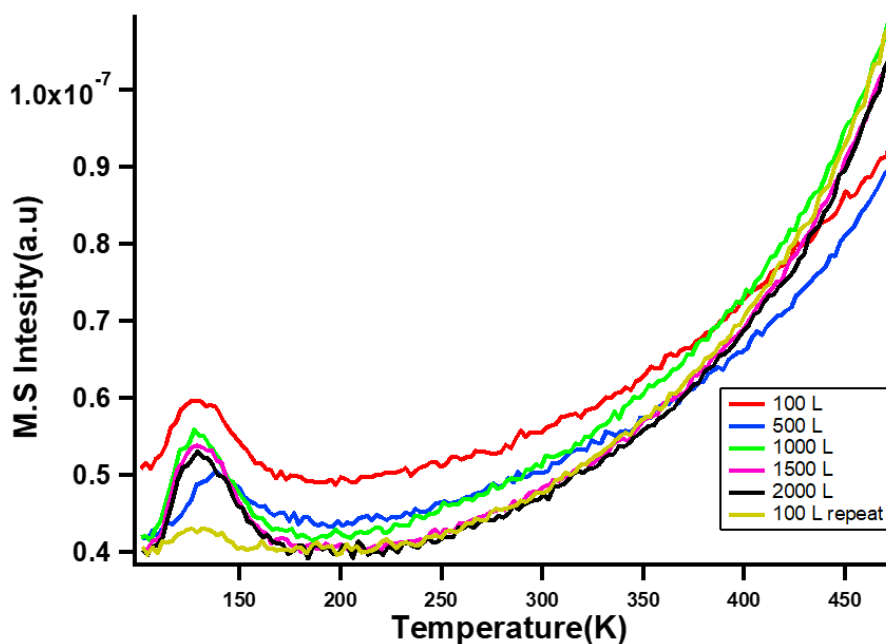


Figure 23 TPD-MS spectra of CO₂ ($m/z = 44$) from DC-4 dosed at 100 K and background pressure of 10^{-9} Torr

- Although the infrared spectra of adsorption of CO₂ on DC-4 suggests promising features (*fig 24*) the spectra could not be interpreted completely and requires further investigations. The two broad peaks, in the infrared adsorption spectra of adsorption, spanning from, $3000\text{ cm}^{-1} - 2500\text{ cm}^{-1}$ and $2700\text{ cm}^{-1} - 2500\text{ cm}^{-1}$ implies that the adsorption of CO₂ on DC-4 causes a change in the framework

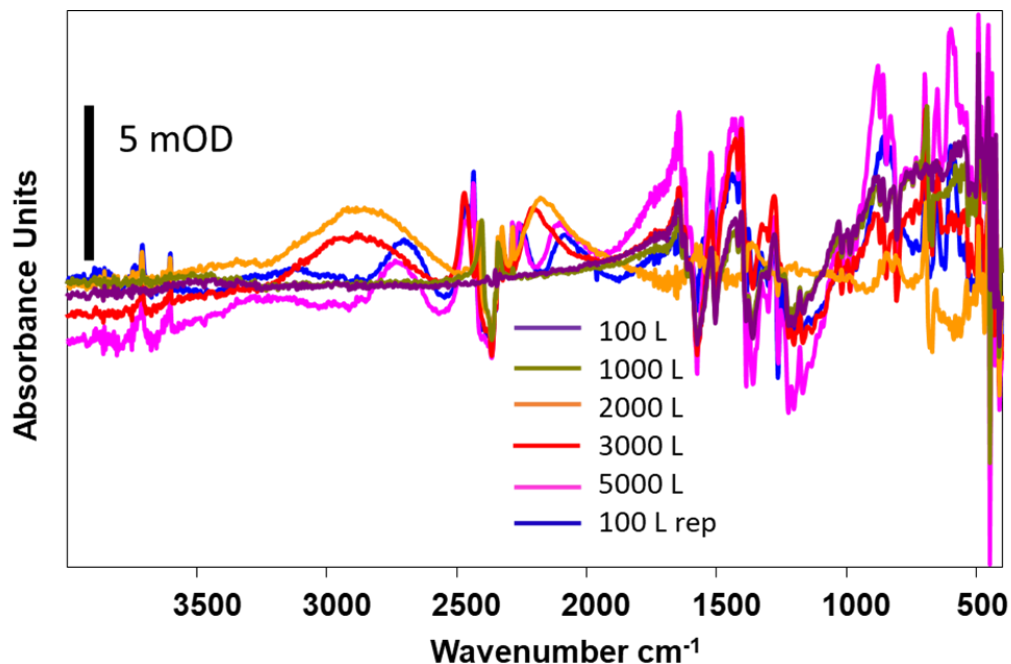


Figure 24 Infrared spectra of adsorption of CO₂ on DC-4 at 100 K, background pressure of 10⁻⁹ Torr

This reasoning is also supported by the infrared spectra taken during desorption of CO₂ and the changes that occurred seem to be irreversible as a function of temperature (fig 25).

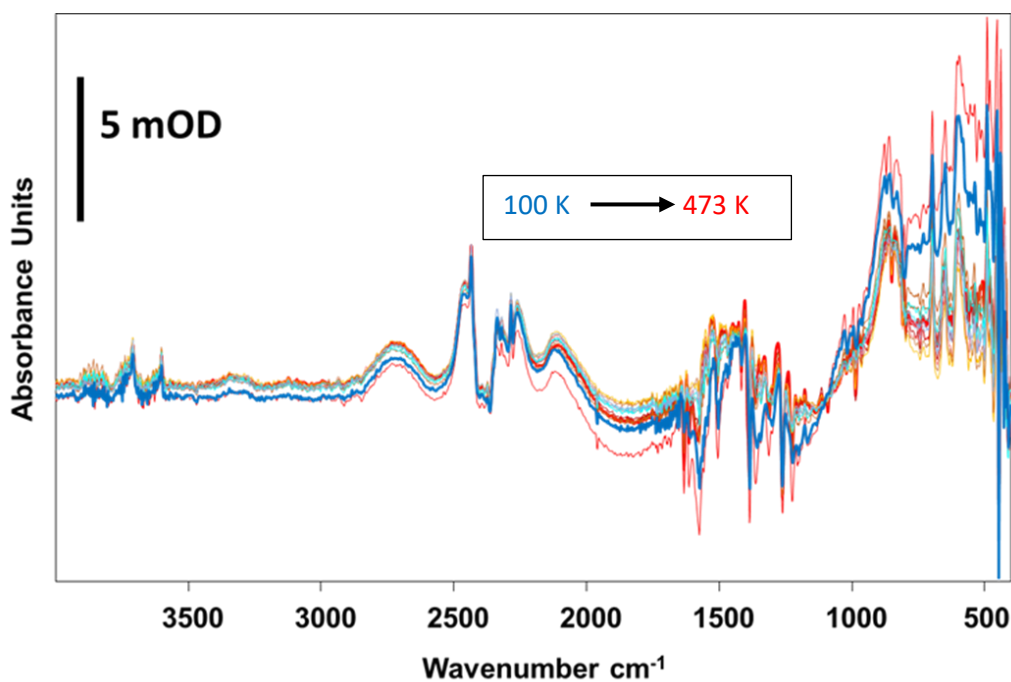


Figure 25 Infrared spectra of temperature programmed desorption of CO₂ from DC-4, dosed at 100 K and background pressure of 10⁻⁹ Torr

The broad peak spanning from 3000 cm^{-1} - 2500 cm^{-1} is absent during desorption and the intensity of peak ranging from 2700 cm^{-1} - 2500 cm^{-1} increases with temperature. These results suggest that

- (a) Surface modifications can occur in DC-4 upon interaction with CO_2 leading to change in vibrational modes of CO_2 and/ or DC-4
- (b) Temperature effects the stability of the framework of DC-4 after adsorption of CO_2

Experiments will be performed to study the surface modifications and address the stability of DC-4 towards CO_2 .

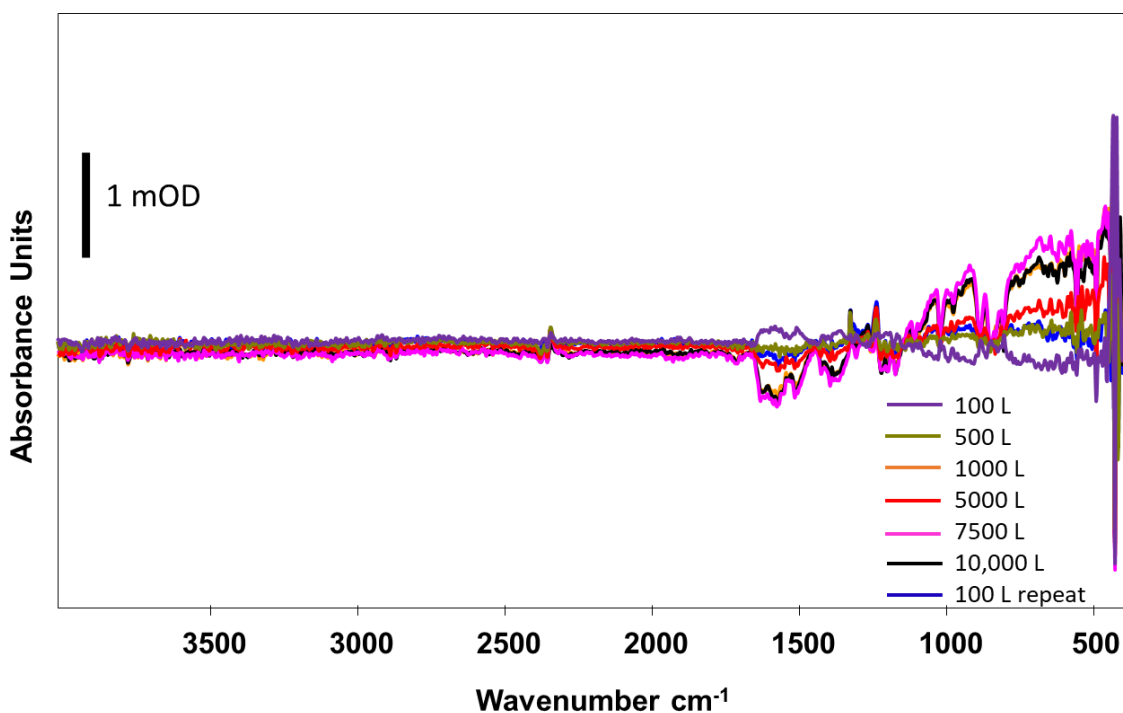


Figure 26 Infrared spectra of adsorption of CO_2 on DC-3 at 100 K, background pressure of 10^{-9} Torr

- **DC-3:** DC-3 shows no evidence of adsorption of CO_2 , which can be seen in the infrared spectra of adsorption (fig 26). The carbonyl stretching at 1700 cm^{-1} is absent in the infrared spectra of adsorption as well as desorption (fig 27) and we suspect that CO_2 has low affinity towards DC-3 compared to DC-4

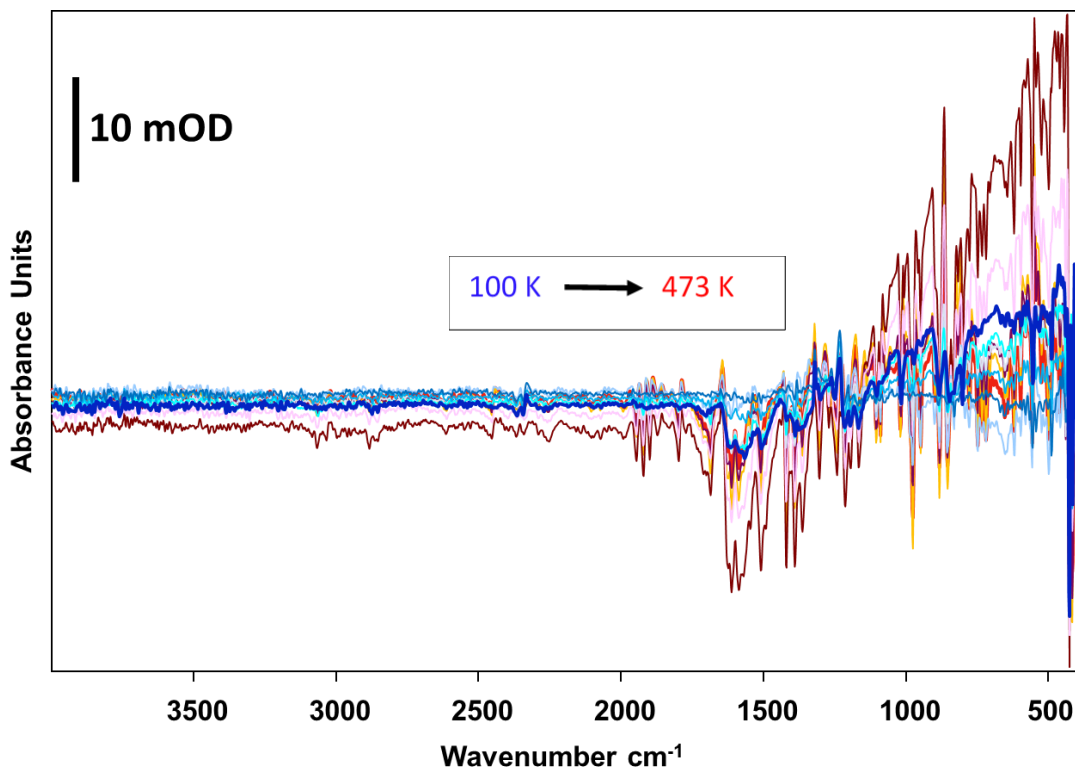


Figure 27 Infrared spectra of temperature programmed desorption of CO₂ from DC-3 dosed at 100 K and background pressure of 10⁻⁹ Torr

Section 3: Nonpolar analytes

Non-polar analytes such as butane, hexane and heptane are chosen for temperature programmed studies. Butane being a small molecule is expected to easily pass through the pores of DC-3, DC-4 (23 Å) while hexane, heptane on the other hand are larger than butane and are expected to be adsorbed more on the surfaces of DC-3, DC-4.

- **DC-3:** The sp^3 C-H stretching at 2900- 3000 cm^{-1} was present in the infrared spectra of adsorption of butane and hexane (fig 28 and fig 29). However, the intensity of sp^3 C-H stretching of butane is lower compared to the intensity of sp^3 C-H stretching of hexane. These results support our hypothesis and suggest that majority of the butane is going into the pores of DC-3.

In the infrared spectra taken during desorption, the peak corresponding to sp^3 C-H stretching of both the analytes (fig 30 and fig 31) decreases with

increase in temperature. At highest temperature the spectrum recovers to the initial spectrum which means that the adsorption of hexane on DC-3 surface is reversible.

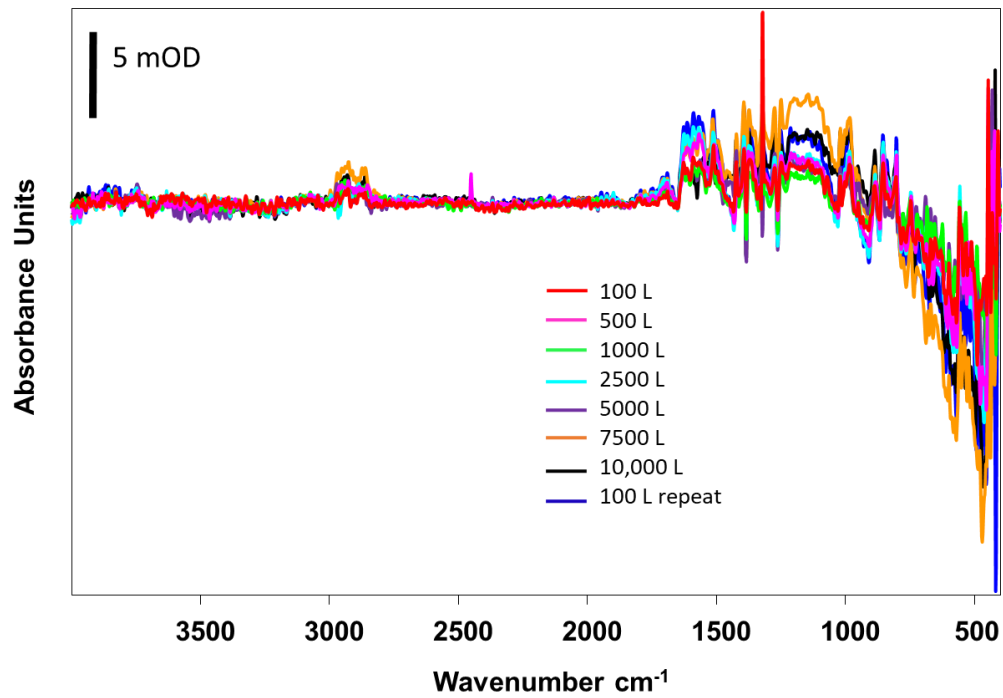


Figure 28 Infrared spectra of adsorption of butane on DC-3 at 100 K, background pressure of 10^{-9} Torr

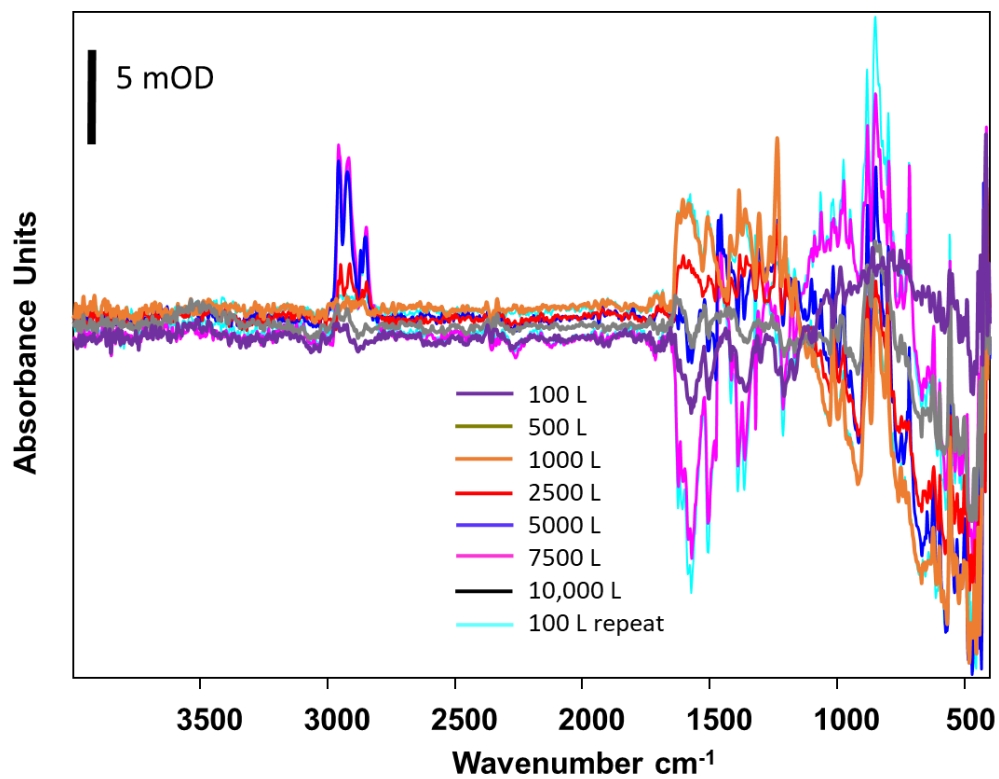


Figure 29 Infrared spectra of adsorption of hexane on DC-3 at 100 K, background pressure of 10^{-9} Torr

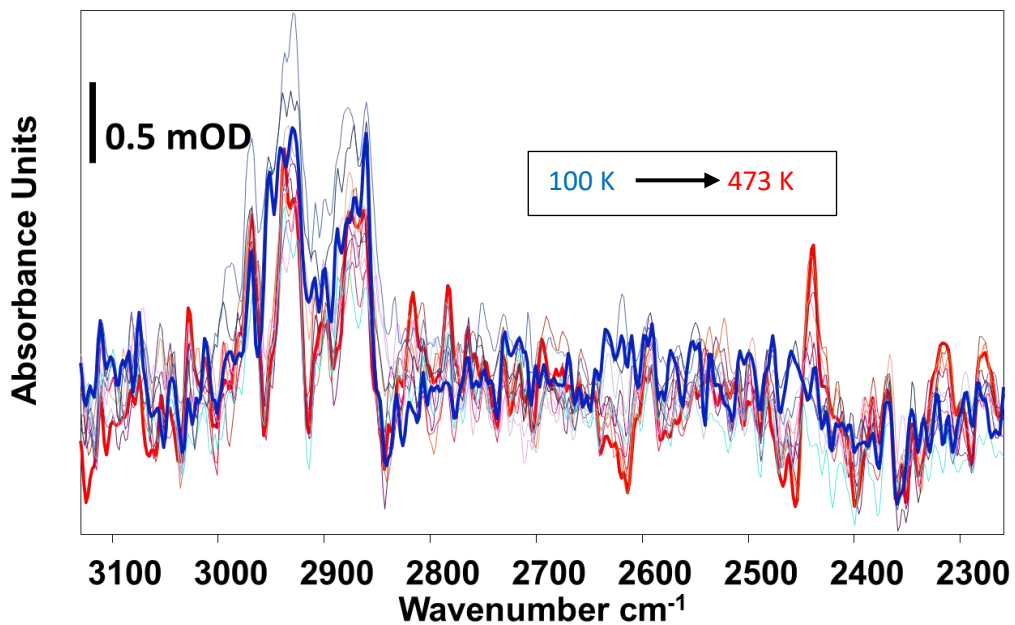


Figure 30 Infrared spectra of temperature programmed desorption of butane from DC-3 dosed at 100 K and background pressure of 10^{-9} Torr

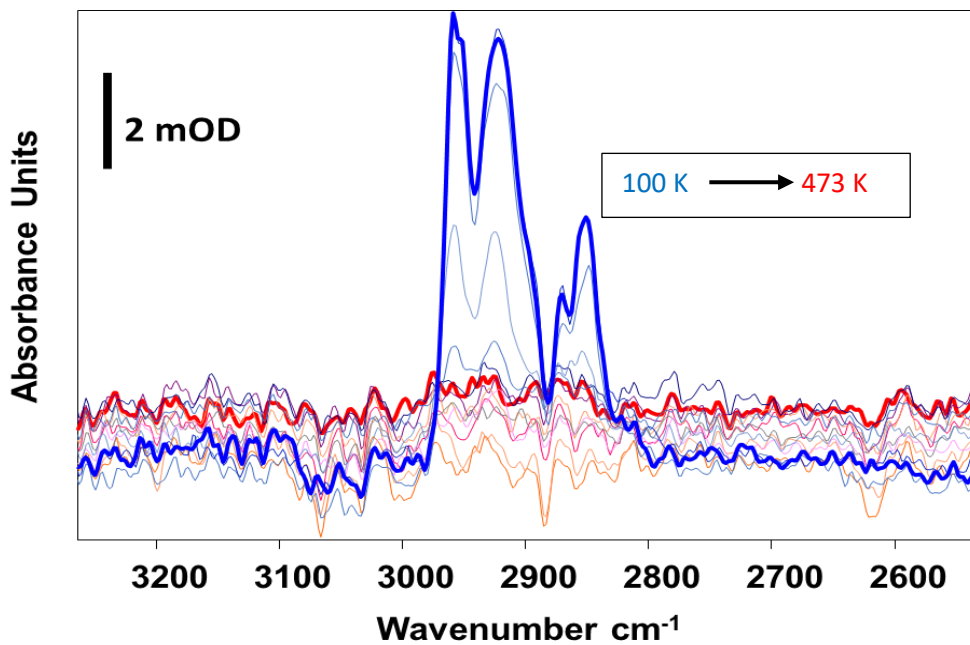


Figure 31 Infrared spectra of temperature programmed desorption of hexane from DC-3, dosed at 100 K and background pressure of 10^{-9} Torr

Interestingly the intensity of sp^3 C-H stretching taken during the desorption of butane increases first and then decreases to same intensity with increase in temperature. We suspect a screening effect for butane adsorption in the framework of DC-3 due to its size but more experiments have to be performed to confirm this.

- **DC-4:** Infrared spectra of adsorption of heptane on DC-4 (fig 32) also shows sp^3 C-H stretching and the peak intensity increases with increased dosing of heptane.

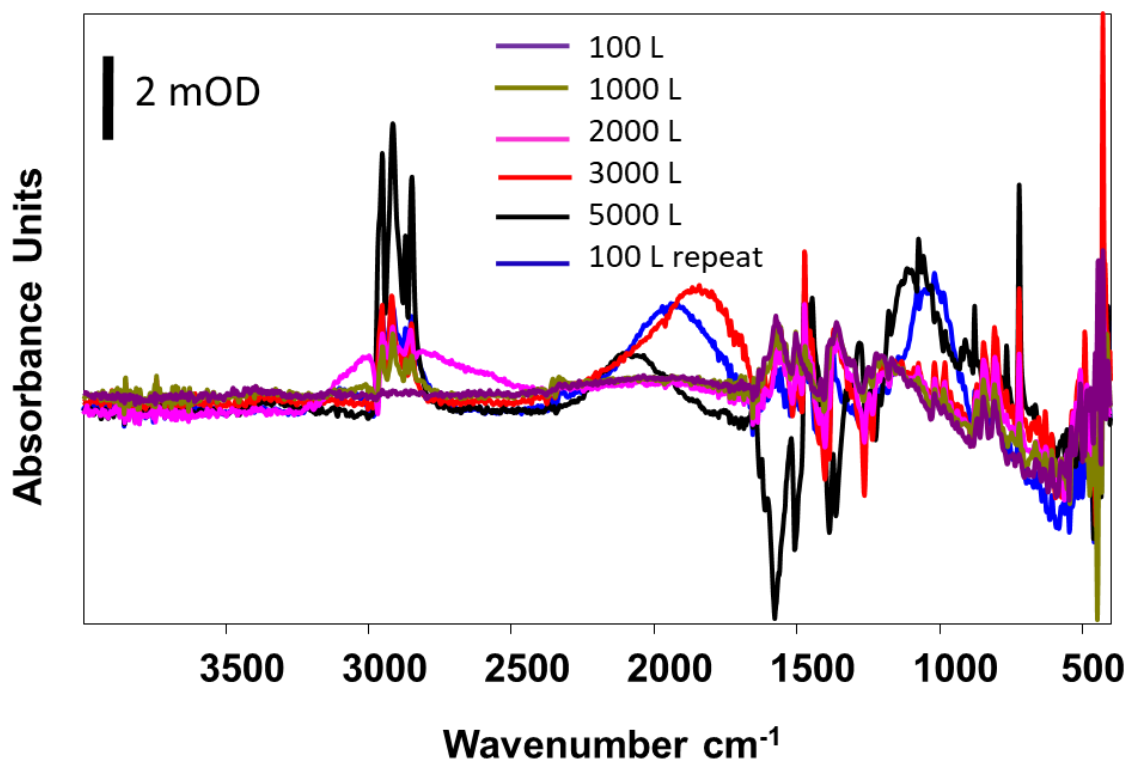


Figure 32 Infrared spectra of adsorption of heptane on DC-4 at 100 K and background pressure of 10^{-9} Torr.

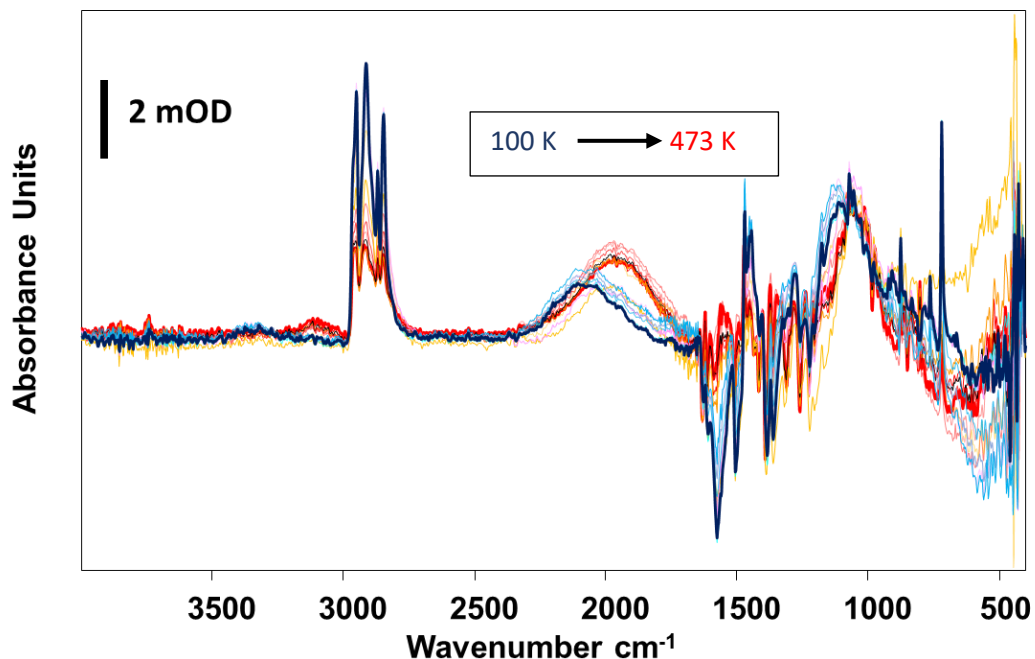


Figure 33 Infrared spectra of temperature programmed desorption of heptane from DC-4, dosed at 100 K and background pressure of 10^{-9} Torr

The infrared spectrum of desorption of heptane (fig 33) shows a decrease in intensity of sp^3 C-H stretching with increase in temperature. However, the broad peaks ranging 2300- 1700 cm^{-1} could not be attributed to any vibrational stretching of either heptane or DC-4 itself. This supports our hypothesis that changes might occur in the framework of DC-4 upon interaction with analytes or increase in temperature.

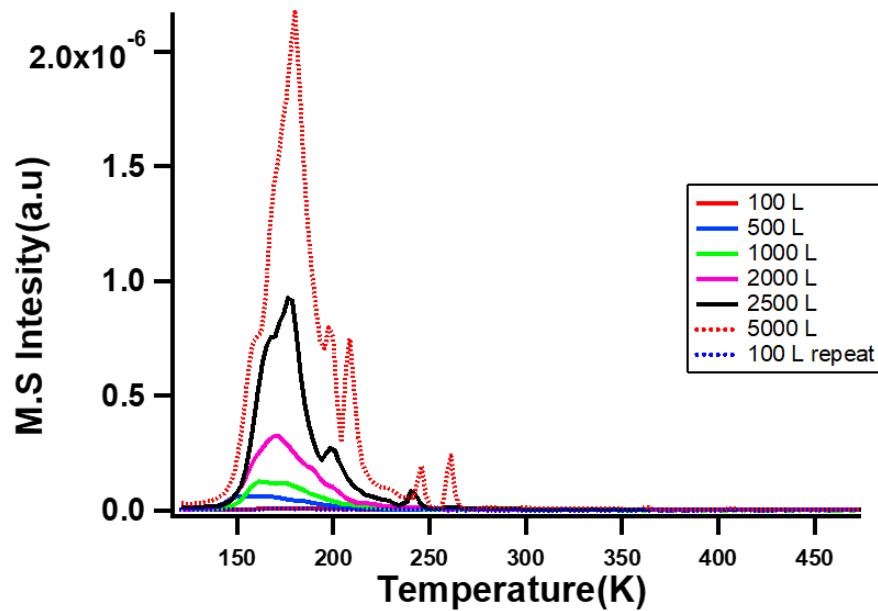


Figure 34 TPD-MS spectra of butane $m/z = 43$ fragment dosed on DC-4 at 123 K and background pressure of 10^{-9} Torr

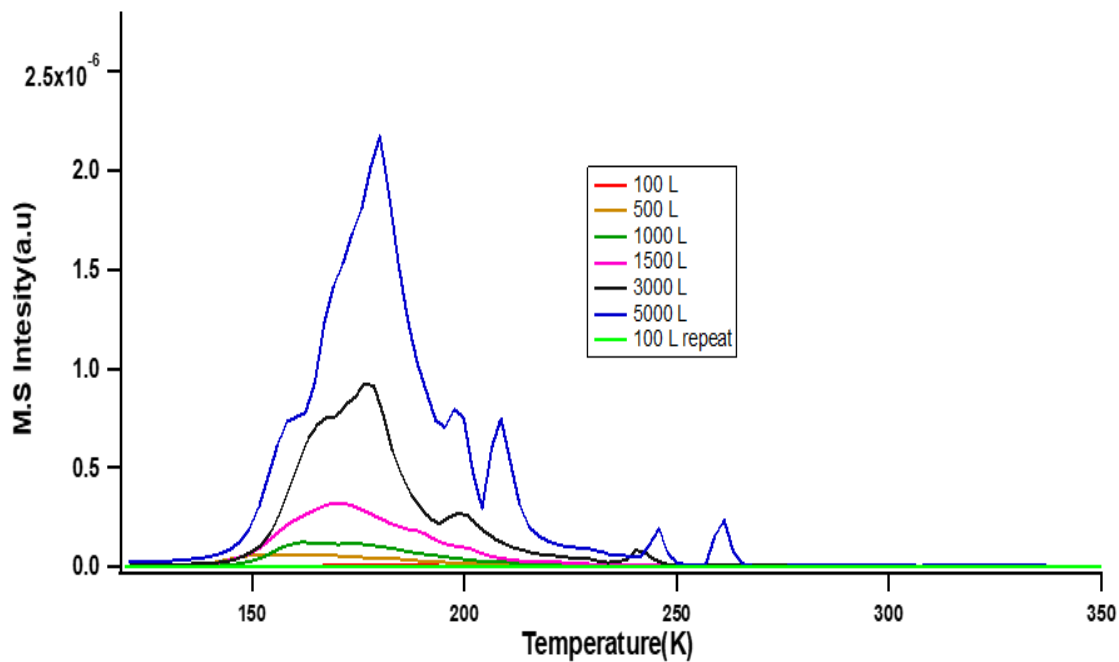


Figure 35 TPD-MS spectra of hexane $m/z = 57$ fragment dosed on DC-4 at 123 K and background pressure of 10^{-9} Torr

Mass spectra taken during temperature programmed desorption of butane (fig 34), hexane (fig 35) from DC-4 are very interesting. Multiple peaks are seen in both cases suggesting multiple binding sites for these molecules. As the dosing of these non-polar gases increases, the number of peaks in the mass spectra

increases which means that multilayer adsorption of butane and hexane is occurring on DC-4. The T_{\max} and energy of desorption are reported in *Table 3*

Analyte	Temperatures of maximum desorption (K)	E_{des} (KJ/mol) calculated using Redhead analysis
Acetone	<ul style="list-style-type: none"> • 155 • 158 • 163 • 178 	<ul style="list-style-type: none"> • 39.5 • 40.3 • 41.7 • 45.6
CO ₂	<ul style="list-style-type: none"> • 126 • 129 • 139 	<ul style="list-style-type: none"> • 31.9 • 32.7 • 35.3
Butane	<ul style="list-style-type: none"> • 159 • 169 • 176 • 198 • 208 • 240 • 245 • 261 	<ul style="list-style-type: none"> • 40.6 • 43.2 • 45.1 • 50.9 • 53.6 • 62.1 • 63.5 • 67.8
Hexane	<ul style="list-style-type: none"> • 168 • 173 • 180 • 202 	<ul style="list-style-type: none"> • 43.0 • 44.3 • 46.2 • 52.0

Table 3 Temperatures of maximum desorption, energies of desorption of acetone, CO₂, butane, hexane from COF DC-4 calculated using Redhead analysis

Chapter 4: Conclusion and future perspectives

In summary we have synthesized boron carbon nitride, with two different approaches, one using lab grade tissue paper as a source of carbon and other by using COF DC-4 as a source of carbon. The former approach did not yield a crystalline, porous BCN but the latter one did.

COFs DC-1, DC-2, DC-3, DC-4, were synthesized and studies on the interactions of COFs DC-3 and DC-4 with various polar, non-polar and industrially relevant analytes of interest, using temperature programmed techniques, were performed.

To the best of our knowledge, this is the first work that reports the usage of TPD surface technique to analyze the interactions of COFs with various analytes.

From the temperature programmed studies we have seen that methanol doesn't interact with DC-3 and DC-4. On the contrary, polar analyte like acetone shows considerable adsorption on DC-3 and DC-4.

CO₂ shows very little desorption from DC-4 evident from the mass spectra taken during desorption. No adsorption or desorption of CO₂ is seen from DC-3 which is clear from the infrared spectra taken during adsorption as well as desorption.

A screening effect is expected when butane interacts adsorbs within the pores of DC-3, whereas hexane and heptane, whose size is more than the pore size of the COFs, adsorb on the surface, interact strongly with the infrared radiation.

The overall performance of DC-3 and DC-4 as sorbents is commendable. However, neat COFs (without any nanoparticles loaded) DC-3 and DC-4 are weak sorbents compared to other porous materials such as MOFs (ref UiO-67), and layered materials (such as CNT and graphite). Hence, as a next step, we plan to load noble metal (Pd) and transition metal nanoparticles (Co, Ni) on these COFs which would increase the number and the diversity of active sites on them. TPD techniques will be exploited to the maximum possible extent to study the interactions of different sized nanoparticles with the analytes of interest and the dependence of adsorption on the cluster size of nanoparticles loaded on the COFs.

Theoretical calculations and simulations for the adsorption on neat COFs as well as metal nanoparticles loaded COFs will be done to support our hypothesis.

Finally, water adsorption and desorption kinetics will be studied using TPD techniques. Our current experimental setup doesn't allow the study and analysis of water as it adsorbs everywhere in the system. However, theoretical modelling and simulations can be done which would guide us and give an insight of the interesting mechanisms that occur in these COFs and suggest which COF would be best suited for temperature programmed studies.

Chapter 5: References and bibliography

1. Geim, A.K. and K.S. Novoselov, *The rise of graphene*. Nature Materials, 2007. **6**: p. 183.
2. Kota, M., N.S. Sharmila, U.V. Waghmare, and C.N.R. Rao, *Composition-dependent photoluminescence and electronic structure of 2-dimensional borocarbonitrides*. Materials Research Express, 2014. **1**(2): p. 025603.
3. Kumar, N., K.S. Subrahmanyam, P. Chaturbedy, K. Raidongia, A. Govindaraj, K. Hembram, A.K. Mishra, U.V. Waghmare, and C.N.R. Rao, *Remarkable Uptake of CO₂ and CH₄ by Graphene-Like Borocarbonitrides, BxCyNz*. Chemsuschem, 2011. **4**(11): p. 1662-1670.
4. kumar, N., K. Moses, K. Pramoda, S.N. Shirodkar, A.K. Mishra, U.V. Waghmare, A. Sundaresan, and C.N.R. Rao, *Borocarbonitrides, BxCyNz*. Journal of Materials Chemistry A, 2013. **1**(19): p. 5806-5821.
5. Ding, S.Y. and W. Wang, *Covalent organic frameworks (COFs): from design to applications*. Chemical Society Reviews, 2013. **42**(2): p. 548-568.
6. Nandi, S., S.K. Singh, D. Mullangi, R. Illathvalappil, L. George, C.P. Vinod, S. Kurungot, and R. Vaidhyanathan, *Low Band Gap Benzimidazole COF Supported Ni₃N as Highly Active OER Catalyst*. Advanced Energy Materials, 2016. **6**(24).
7. Mullangi, D., S. Nandi, S. Shalini, S. Sreedhala, C.P. Vinod, and R. Vaidhyanathan, *Pd loaded amphiphilic COF as catalyst for multi-fold Heck reactions, C-C couplings and CO oxidation*. Scientific Reports, 2015. **5**.
8. Graham, J.D. and N.I. Hammer, *Photocatalytic Water Splitting and Carbon Dioxide Reduction*, in *Handbook of Climate Change Mitigation*, W.-Y. Chen, et al., Editors. 2012, Springer US: New York, NY. p. 1755-1780.
9. Schneider, J., M. Matsuoka, M. Takeuchi, J. Zhang, Y. Horiuchi, M. Anpo, and D.W. Bahnemann, *Understanding TiO₂ Photocatalysis: Mechanisms and Materials*. Chemical Reviews, 2014. **114**(19): p. 9919-9986.
10. Chhetri, M., S. Maitra, H. Chakraborty, U.V. Waghmare, and C.N.R. Rao, *Superior performance of borocarbonitrides, BxCyNz, as stable, low-cost metal-free electrocatalysts for the hydrogen evolution reaction*. Energy & Environmental Science, 2016. **9**(1): p. 95-101.
11. Li, Z., X. Meng, and Z. Zhang, *Recent development on MoS₂-based photocatalysis: A review*. Journal of Photochemistry and Photobiology C: Photochemistry Reviews, 2018. **35**: p. 39-55.
12. Kang, Q., L. Vernisse, R.C. Remsing, A.C. Thenuwara, S.L. Shumlas, I.G. McKendry, M.L. Klein, E. Borguet, M.J. Zdilla, and D.R. Strongin, *Effect of Interlayer Spacing on the Activity of Layered Manganese Oxide Bilayer Catalysts for the Oxygen Evolution Reaction*. Journal of the American Chemical Society, 2017. **139**(5): p. 1863-1870.
13. Pramoda, K., M.M. Ayyub, N.K. Singh, M. Chhetri, U. Gupta, A. Soni, and C.N.R. Rao, *Covalently Bonded MoS₂-Borocarbonitride Nanocomposites Generated by Using Surface Functionalities on the Nanosheets and Their Remarkable HER Activity*. The Journal of Physical Chemistry C, 2017.

14. Atkins, P.W. and J. De Paula, *Atkins' physical chemistry*. 2011, Oxford: Oxford University Press.
15. Yates Jr, J.T., *Experimental Innovations in Surface Science*. Springer : New York, . 2015.
16. Fitzgerald, S.A., K. Shinbrough, K.H. Rigdon, J.L.C. Rowsell, M.T. Kapelewski, S.H. Pang, K.V. Lawler, and P.M. Forster, *Temperature-Programmed Desorption for Isotope Separation in Nanoporous Materials*. The Journal of Physical Chemistry C, 2018. **122**(4): p. 1995-2001.
17. Kazachkin, D., Y. Nishimura, S. Irle, K. Morokuma, R.D. Vidic, and E. Borguet, *Interaction of acetone with single wall carbon nanotubes at cryogenic temperatures: A combined temperature programmed desorption and theoretical study*. Langmuir, 2008. **24**(15): p. 7848-7856.
18. Kwon, S., R. Vidic, and E. Borguet, *Enhancement of adsorption on graphite (HOPG) by modification of surface chemical functionality and morphology*. Carbon, 2002. **40**(13): p. 2351-2358.
19. Kazachkin, D.V., Y. Nishimura, H.A. Witek, S. Irle, and E. Borguet, *Dramatic Reduction of IR Vibrational Cross Sections of Molecules Encapsulated in Carbon Nanotubes*. Journal of the American Chemical Society, 2011. **133**(21): p. 8191-8198.
20. Dejong, A.M. and J.W. Niemantsverdriet, *THERMAL-DESORPTION ANALYSIS - COMPARATIVE TEST OF 10 COMMONLY APPLIED PROCEDURES*. Surface Science, 1990. **233**(3): p. 355-365.

Chapter 6: Appendix

Infrared spectra of DC-3 and DC-4 coated on tungsten mesh, used as a reference for spectrum subtraction.

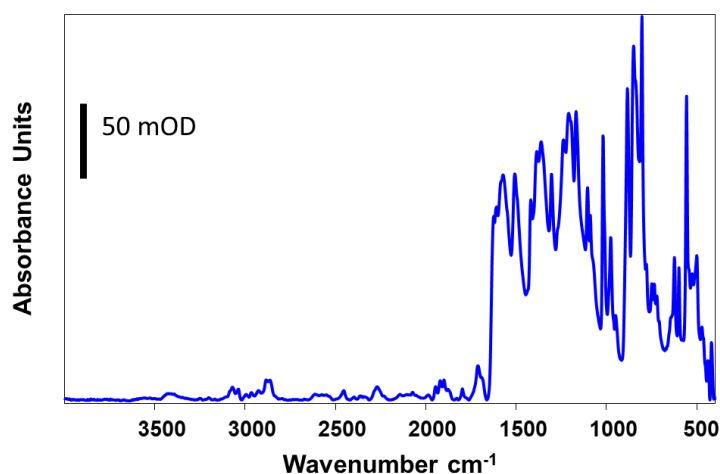


Figure 36 Infrared spectra of DC-3 on tungsten mesh, used as reference spectra for subtraction, taken at 100 K and base pressure of 10^{-9} Torr

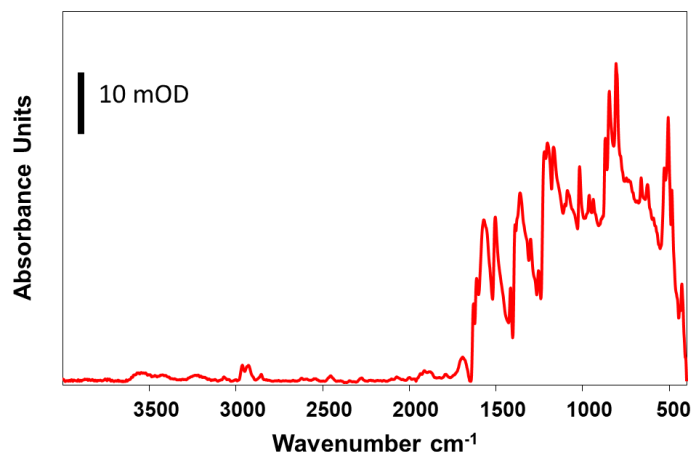


Figure 37 Infrared spectra of DC-4 on tungsten mesh, used as reference spectra for subtraction, taken at 100 K and base pressure of 10^{-9} Torr

Calculation of dosage of analyte from adsorption

Adsorption of any analyte is done by plotting the total pressure (Torr) of the system vs time (sec) for which the dosing is performed. One Langmuir (1L) = 10^{-6} Torr-sec. Hence the area under the graph of total pressure (Torr) vs time (sec) when divided by 10^{-6} Torr-sec gives us the dosing amount of the analyte in the units of Langmuir.

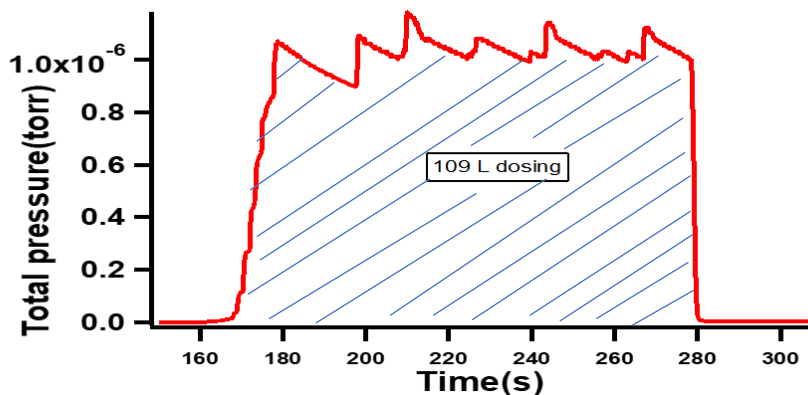


Figure 38 An example of adsorption of 109 L dosing of an analyte at temperature 110 K and base pressure of 10^{-9} Torr

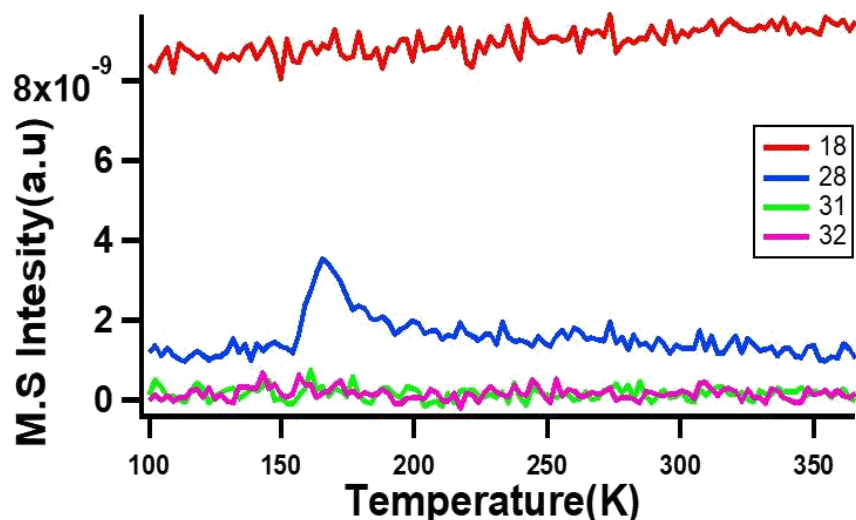


Figure 39 Desorption of MeOH from DC-4, dosed at 110 K and base pressure of 10^{-9} Torr

Redhead analysis

Redhead analysis is employed to calculate the energies of desorption of the analytes.

We have referred to the paper [20] and calculated the energies of desorption of analytes from DC-3 and DC-4.

Rate of thermal desorption is an Arrhenius process and is determined in terms of Polanyi- Wigner equation (fig 40)

$$-\frac{d\theta}{dT} = \frac{A}{\beta} \theta^n \exp\left(\frac{-\Delta E_{des}}{RT}\right)$$

Figure 40 Polanyi-Wigner equation to determine rate of thermal desorption

Where,

T: Temperature; A: Pre-exponential (frequency) factor (s^{-1}); β : Heating rate ($K.s^{-1}$); θ : Surface coverage; n: Kinetic order of desorption; R: Gas constant ($8.314 J.mol^{-1}.K^{-1}$)

There are a few assumptions made in the Redhead analysis model of desorption, which yields a simple relation between T_{max} , energy of desorption and pre-exponential factor, which are:

- a. Kinetics parameters of desorption are independent of surface coverage
- b. Desorption follows first order kinetics

Incorporating the above conditions, the relation between T_{max} , energy of desorption and pre-exponential factor is derived

$$\Delta E_{des} = RT_{max} \left[\ln \frac{A T_{max}}{\beta} - \ln \frac{\Delta E_{des}}{RT_{max}} \right]$$

commonly chosen value
 $A = 10^{13} \text{ s}^{-1}$
Estimated as ~ 3.46

Figure 41 Final equation of Redhead analysis used to calculate the energy of desorption

Frequency factor A is chosen to be 10^{13} s^{-1} and the 2nd term in the parentheses is taken as 3.46. Using the above equation energy of desorption are calculated within 1.5% error range of the accepted values.